Definição de estilo: Hiperligação

Modeling impacts of ozone on gross primary production across

European forest ecosystems using JULES

- Inês Vieira^{1*}, Félicien Meunier^{1,2}, Maria Carolina Duran Rojas³, Stephen Sitch³, Flossie Brown⁴,
- 4 Giacomo Gerosa⁵, Silvano Fares⁶, Pascal Boeckx², Marijn Bauters¹ and Hans Verbeeck¹
- 1 Q-ForestLab, Laboratory of Quantitative Forest Ecosystem Science, Department of Environment, Ghent University, Gent,
 Relgium
- 8 ²ISOFYS, Isotope Bioscience Laboratory, Department of Green Chemistry and Technology, Ghent University, Gent, Belgium
- 9 ³ Faculty of Environment, Science & Economy, University of Exeter, Exeter, United Kingdom
- 10 ⁴ Institute for Atmospheric and Climate Science, ETH Zurich, Zurich, Switzerland
- 11 ⁵ Faculty of Mathematical, Physical and Natural Sciences, Università Cattolica del Sacro Cuore, Brescia, Italy
- 12 6 Institute for Agriculture and Forestry Systems in the Mediterranean, National Research Council of Italy, Naples, Italy
- 13 Correspondence to: Inês Vieira (ines.dossantosvieira@ugent.be)

- 14 **Abstract.** This study investigates the effects of tropospheric ozone (O₃), a potent greenhouse gas and air pollutant, on European
- 15 forests, an issue lacking comprehensive analysis at the site level. Unlike other greenhouse gases, Os in the
 - tropospheretropospheric O₃ is primarily formed through photochemical reactions, and it significantly impairing impairs
- 17 vegetation productivity and carbon fixation, thereby impacting affecting forest health and ecosystem services. We utilise data
- 18 from multiple European flux tower sites and integrate statistical and mechanistic modelling approaches to simulate O₃ impacts
- 19 on photosynthesis and stomatal conductance. The study examines six key forest sites across Europe: Hyytiälä and Värriö
- 20 (Finland), Brasschaat (Belgium), Fontainebleau-Barbeau (France), Bosco-Fontana, and Castelporziano 2 (Italy), representing
- 21 boreal, temperate, and Mediterranean climates. These sites provide a diverse range of environmental conditions and forest
- 22 types, enabling a comprehensive assessment of O3 effects on Gross Primary Production (GPP). We calibrated the Joint UK
- 23 Land Environment Simulator (JULES) model using observed GPP data to simulate different O₃ exposure sensitivities.
- 24 Incorporating O₃ effects improved the model's accuracy across all sites, although the magnitude of improvement varied
- 25 depending on site-specific factors such as vegetation type, climate, and ozone exposure levels. The GPP reduction due to ozone
- 26 exposure varied considerably across sites, with annual mean reductions ranging from 1.04% at Värriö to 6.2% at Bosco-
- 27 Fontana. These findings emphasise the need to account for local environmental conditions when assessing ozone stress on
- 28 forests. This study highlights thekey model strengths and limitations of the JULES model in representing Q3-Q3-vegetation
- 29 interactions, providing critical insights with implications for predicting improving forest health and productivity simulations

under future air pollution scenarios. The model effectively captures the diurnal and seasonal variability of GPP and its sensitivity to O₃ stress, particularly in boreal and temperate forests. However, its performance is limited in Mediterranean ecosystems, where pronounced O₃ peaks and environmental stressors such as high vapor pressure deficit exacerbate GPP declines, pointing to the need for improved parameterisation and representation of site-specific processes. By integrating in situ measurements, this research contributes to developing targeted strategies for mitigating the adverse effects of O₃ on forest ecosystems.

1 Introduction

30

31

32

33

34

35

36

37

38

39

40

41

42

43

44

45

46

47

48

49

50

51

52

53

54

55

56

57

58

59

60

61

Ground-level ozone (O3) is a greenhouse gas and an air pollutant with a strong oxidative capacity being responsible for negatively impacting human health (Nuvolone et al., 2018; Lu and Yao, 2023), water and carbon cycles (Sitch et al., 2007; Lombardozzi et al., 2015), agriculture and crop production (Van Dingenen et al., 2009; Feng et al., 2022; Li et al., 2022) and vegetation productivity (Ainsworth et al., 2012; Yue and Unger, 2014; Ainsworth et al., 2019; Savi et al., 2020). In the troposphere, O₃ is not emitted directly, contrary to other greenhouse gases, such as carbon dioxide (CO₂) and methane (CH₄). The majority of O₃ (about 90%) is generated by the photochemical oxidation of its precursor gases (natural and anthropogenic), such as CH₄, carbon monoxide (CO), and volatile carbon compounds (VOCs) in the presence of nitrogen oxides (NOx). The remaining 10% is from the influx of ozone from the stratosphere. On the other hand, tropospheric O₃ is primarily removed through chemical destruction and dry deposition to terrestrial surfaces that occurs via stomatal (Fowler et al., 2009; Ducker et al., 2018; Clifton et al., 2020) and non-stomatal pathways (Zhang et al., 2003; Wong et al., 2022). Stomatal O₃ uptake damages vegetation by causing cell death and decreasing carbon fixation (Li et al., 2019), which in turn leads to reduced productivity (Ainsworth et al., 2012) and early senescence (Gielen et al., 2007). In particular, it reduces gross primary production (GPP), the gross carbon uptake via photosynthesis, a measure of ecosystem productivity (Proietti et al., 2016; Cailleret et al., 2018; Grulke et al., 2019). Exposure to O3 leads to reductions in photosynthesis and stomatal conductance, thereby decreasing both gross primary productivity (GPP) and transpiration. These physiological impacts have broader consequences for climate, including reduced carbon uptake, decreased latent heat flux (LE), and diminished water vapour release. Additionally, lower stomatal conductance reduces dry deposition of ozone, which can exacerbate near-surface ozone concentrations. Therefore, incorporating a representation of ozone damage to plants in land surface and Earth System models (LSMs and ESMs) is essential because many regions experience potentially damaging $\Theta_3 O_3$ concentrations. However, while most studies agree that Θ_2O_3 exposure results in significant reductions in GPP, the reduction varies with measurement location or assumptions used in the models. For example, Sitch et al. (2007) predicted a decline in global GPP of 14 to 23% by 2100. Lombardozzi et al. (2015) predicted a 10.8% decrease in present-day (2002-2009) GPP globally. Also Similarly, Yue and Unger (2014) foundreported that O₃ozone damage decreases reduced GPP by 4% 8% on an average in of 4-8% across the eastern US, leading to significant United States, with localised reductions reaching as high as 11 % _17 % decreases on % along the east coast.

| Formatou: Não Superior à linha/ Inferior à linha |
|--|
| Formatou |

high solar radiation intensifies O₃ formation due to interactions between traffic and anthropogenic emissions—mainly from traffic and industrial activities activity—enhance photochemical O₃ formation (Sicard et al., 2021). Currently, the European standard used to protect vegetation against negative impacts of O₃ is the Accumulated Ozone over a Threshold of 40 ppb (AOT40), i.e. the cumulative exposure to hourly O₃ concentrations above 40 ppb over the daylight hours of the growing season (Anav et al., 2017; Proietti et al., 2021). However, the O₃ uptake through stomata is a better metric for assessing plant damage because it estimates the actual quantity of O₃ entering the leaf tissues (Anav et al., 2016; Sicard et al., 2016). High ambient O₃ levels may not damage plants when drought and/or other environmental stressors limit the stomatal aperture (Shang et al., 2024). Therefore, flux-based approaches were developed to assess the effects of O3 on vegetation. This method quantifies leaf O₃ uptake and the dose that actually enters the plant tissue via stomata and considers the environmental constraints that may limit optimal stomatal conductance. For example, Proietti et al. (2016) performed a comprehensive study on 37 European forest sites during the period of 2000-2010 to assess surface O₃ effects on GPP. In this study, the DO₃SE (Deposition of O₃ and Stomatal Exchange) model (Emberson et al., 2001) was used to estimate ozone uptake/stomatal ozone flux using the Jarvis multiplicative method for stomatal conductance (Jarvis, 1976). The results showed that GPP was reduced between 0.4% and 30% annually across different sites. Also, Anav et al. (2011) showed, using a land surface model coupled with a chemistry transport model, a 22% reduction in yearly GPP and a 15-20% reduction in leaf area index (LAI) due to O₃ exposure, with the most substantial impacts occurring during the summer months. Interestingly, not all studies have found significant negative effects of O₃ on GPP. For instance, research on a Scots pine stand in Belgium over 15 years found no significant O₃ effects on GPP despite high stomatal O₃ uptake (Verryckt et al., 2017). This suggests that the impact of O₃ may vary depending on specific forest types (Sorrentino et al., 2025) and local conditions. (Lin et al., 2019; Otu-Larbi et al. 2020). Satellite observations have also been utilised to assess O3-induced GPP reductions, estimating a decrease of 0.4-9.6% across European forests from 2003-2015. These findings align with previous estimates and highlight soil moisture as a critical interacting variable influencing GPP reductions, particularly in Mediterranean regions (Vargas et al., 2013). Therefore, while the negative effects of O₃ on GPP in European forests are well-documented, the extent of these impacts can vary significantly based on regional conditions, forest types, methodological approaches, and it is not clear what drives the local differences. Understanding these variations is crucial for accurately assessing the broader implications of O₃ on forest productivity and ecosystem services. This gap in the literature underscores the need for detailed studies that evaluate the influence of ozone on forest productivity in Europe using advanced process-based models. This study provides a detailed, site-level analysis of O3 impacts on GPP across European forests, leveraging local in situ measurements of O₃, CO₂ exchange, and meteorological data to optimise the Joint UK Land Environment Simulator (JULES) model. Our objectives are to quantify O3-induced GPP limitations and assess model improvements through the incorporation of ozone damage mechanisms. Specifically, we aim to address the following research questions:

In Europe, surface O₃ pollution poses a significant challenge to air quality-challenge, particularly in southern Europe, where

62

63

64

65

66

67

68

69

70

71

72

73

74

75

76

77

78

79

80

81

82

83

84

85

86

87

88

89

90

91

92

93

94

95

1. To what extent can we improve GPP simulations for European forests of a process-based model by incorporating plant sensitivity to ozone?

- 2. To what extent does ozone limit GPP across European forests?
- 3. How do ozone impacts interact with other environmental factors, and how can an optimised model help us understand these mechanisms, particularly on high-ozone days?

To achieve these objectives, we combined a multi-year eddy covariance flux tower dataset across a latitudinal gradient in Europe across six sites in boreal, temperate, and Mediterranean forests and statistical and process-based models, providing a comprehensive understanding of ozone's effects on GPP.

2 Materials and Methods

2.1 Study Area

96

97

98

99

100

101

102

103

104

105106

107

108

109

110

111

112

113

114

115

116117

118

119

120

121

122

123

124

125

We investigated six sites along a European latitudinal gradient in four countries: Finland, Belgium, France and Italy (Fig. 1, Table 1), belonging to the Integrated Carbon Observation System (ICOS, https://www.icos-cp.eu/, last access: 20 September 2024). These sites span boreal, temperate, and Mediterranean climates, representing diverse forest ecosystems with varying ozone exposure, productivity, and environmental conditions.

The Värriö site (FI-Var) of the University of Helsinki is located in Värriö strict nature reserve, Salla, Finnish Lapland. The area lies 130 km north of the Arctic Circle and 6 km from the Finnish Russian border. The flux tower is located at the arcticalpine timberline on the top plateau of the hill of Kotovaara, at 395 m a.s.l, and surrounded by a homogeneous and relatively open 10m tall Scots Pine (Pinus sylvestris L.) forest. The leaf area index (LAI) varies between 0.0013 and 0.68 m²m⁻² (Dengel et al., 2013). The Hyytiälä forest (FI-Hyy) boreal site is located 220 km NW from Helsinki, Finland. The station is dominated by Scots pine (Pinus sylvestris L.), Norway spruce, and birch on a slightly hilly terrain. The LAI varies between 0.45 and 3.04 m²m⁻² (Schraik et al., 2023). The Brasschaat site (BE-Bra) is a forest located 20 km northeast of Antwerp, Belgium. The study site consists of a 150-ha mixed coniferous/deciduous forest dominated by Scots pine. The LAI varies between 1 and 1.5 m²m⁻ ² (Op de Beeck et al., 2010). Fontainebleau-Barbeau forest (FR-Fon) is located 53 km southeast of Paris, France. Fontainebleau-Barbeau is a deciduous forest mainly composed of mature sessile oak (Quercus petraea (Matt.) Liebl). The average LAI over the 2012-2018 period was 5.8 m²m⁻², ranging from 4.6 to 6.8 m²m⁻² (Soudani et al., 2021). The Bosco-Fontana site (IT-BFt) is a 233-ha forest composed mainly of mature Oak-Hornbeam (Carpinus betulus) at Po Valley, a few kilometres from Mantova, Italy. The LAI ranges between 0.9 and 3.0 m2m2 (Gerosa et al., 2022). The Castelporziano 2 site (IT-Cp2) is located in the Presidential Estate of Castelporziano, around 25 km southwest of the centre of Rome, Italy. Castelporziano covers an area of about 6000 ha of undisturbed Mediterranean maquis, oak and pine forests. The experimental site is located inside a pure Holm Oak (Quercus ilex) stand with some shrubs in the understory. The LAI varies between 0.5 and 4.5 m²m⁻² (Gratani and Crescente, 2000). More details about each site are available in Table 1.

| 26 | Table | 1: | Overview | of the | study s | sites. |
|----|-------|----|----------|--------|---------|--------|
|----|-------|----|----------|--------|---------|--------|

| | 7 | | | | iälä | | schaat | 1.011 | tainebl | cau- | Bosco | | Castelporzian | |
|-----------------|--------------------------|-----------------------------|-------------------------|-------------------------------|-------------|----------------|-------------------|--------------------|------------|--------------------|------------|----------------------|---------------|-------|
| | | Värr | iö | | | | Barbeau Fontana 2 | | 2 | | | | | |
| | | | | | | BE-Bra | | | | | | | | |
| Aanan | I | FI-Va | | FI-Hy | | | | ra FR-Fon | | n IT-BFt | | | ITT. C.: 2 | |
| Acron | iyiii i | ri-va | I.I. | гі-пу | /y | DE-D | ıd | rk- | ron | | II-DFL | | IT-Cp2 | |
| 1 | Country | ountry Finland Finla | | Finland | land Belgiu | | ım France | | Italy | | Italy | | | |
| | Latitude 67.75 61 | | 61.85 | | 51.30 | | 48.47 | | 45.19 | | 41.70 | | | |
| _ | (°) | | | | | | | | | | | | | |
| , | Y | | 20.61 | | 24.20 | | 4.52 | | 2.78 | | 1074 | | 12.26 | |
| _ | Longitu e (°) | ıa | 29.61 | | 24.29 | | 4.52 | | 2.78 | | 10.74 | | 12.36 | |
| | | | | | | | | | | | | | | |
| Elevati | on (m | 395 | 5 | 181 | 1 | 16 | | 103 | | 23 | | 19 | | |
| a.s.l.) | | | | | | | | | | | | | | |
| Köpper | <u>n-</u> | Sub | <u>oarctic</u> | Sub | oarctic . | Ma | <u>rine</u> | Mar | <u>ine</u> | Hun | <u>nid</u> | Hot | -summer | |
| <u>Geiger</u> | | | | (Df | (Dfc) | | <u>st</u> | | | <u>subtropical</u> | | <u>Mediterranean</u> | | |
| <u>classifi</u> | cation | | | | | coast (Cfb) | | (Cfb) | | (Cfa | (Cfa) | | (Csa) | |
| | | | | | | <u>[CI</u> | <u>nì</u> | | | | | | | |
| Forest (| type | | ergreen | | ergreen | | ĸed | | iduous | | duous | | rgreen Broad | lleaf |
| | | | edleleaf | | edleleaf | For | ests | | adleaf | | ıdleaf | For | est | |
| | | For | ests | For | ests | | | Fore | ests | Forests | | | | |
| J | Meteor | ol | 2017- | | 1996- | | 1996- | | 2005- | | 2013- | | 2012- | |
| | ogical | | 2023 | | present | t | presen | present present 20 | | 2020 | | present | | |
| 9 | dataset | | | | | | | | | | | | | |
| 03 | 3 | | 2017- 1996- 1996- 2014- | | 4- | 2013 | - | 2013- | | | | | | |
| co | ncentra | centration 2023 present | | ent | 2020 |) | 2020 | 0 | 2020 | | 2014 | | | |
| | Fluxes | | 2017- | 2017- 1996- 1999- 2005- 2012- | | | 2012- | | | | | | | |
| - | (GPP, L | E) | 2023 | | present | t | presen | t | preser | ıt | presen | t | present | |
| B.4 | Iean | | -0.5 | | 3.5 | | 10.5 | | 11.4 | | 14.5 | | 16.43 | _ |
| A | nnual | | -0.5 | | 3.3 | | 10.5 | | 11.4 | | 14.5 | | 10.43 | |

| Formatada | |
|------------------|--|
| Formatou | |
| Formatou | |
| Formatou | |
| Formatada | |
| Formatou | |
| Formatou | |
| Formatou | |
| Formatou | |
| Formatada | |
| Formatou | |
| Formatada | |
| Formatada | |
| Formatada | |
| Formatou | |
| Formatada | |
| Tabela Formatada | |
| Formatou | |
| Formatada | |
| Formatou | |
| Formatada | |
| Tabela Formatada | |
| Formatou | |
| Formatada | |
| Formatou | |
| Formatada | |
| Formatou | |
| Formatada | |
| Tabela Formatada | |
| Formatou | |
| Formatou | |
| Formatou | |
| Formatada | |
| Formatou | |
| Formatada | |
| Tabela Formatada | |
| Formatou | |

Formatada

| temperature (°C) | | | | | | |
|--|------------|-------------|------------------|------------------|------------|------------|
| Mean | 601.0 | 711.0 | 920.7 | 678.9 | 697.0 | 601.0 |
| annual precipitat ion (mm) | 601.0 | 711.0 | 920.7 | 678.9 | 697.0 | 601.0 |
| Mean annual | 31.85 | 28.37 | 23.78 | 30.08 | 34.47 | 27.72 |
| 03 | 01.00 | 20.07 | 20.70 | 00.00 | 0 11 17 | |
| concentration (ppb) | 1 | | | | | |
| Maximum | 109.57 | 89.32 | 143.0 | 139.25 | 144.71 | 119.84 |
| O3, concentra tion (ppb) | | | | | | |
| Mean | 336.96 | 1538.42 | | 41912.28 | 20084.90 | 13172.03 |
| summer AOT40 (ppb.hours) | | | 5406.77 | | | |
| Mean | 28.37 | 32.17 | 31.67 | 71.71 | 42.30 | 45.98 |
| summer 03 (ppb) | | | | | | |
| Mean annual GPP (tC ha ⁻¹ yr ⁻¹) | 470.1 | 470.1 | 1181 | 1452.9 | 2069.3 | 1683.6 |
| Peak LAI | 0.68 | 3.04 | 1.31 (Op | 6.8 | 3.0 | 4.76 |
| (m2m-2) | (Dengel et | (Schraik et | | (Soudani | (Gerosa et | (Fares et |
| | al., 2013) | al., 2023) | et al., 2010) | et al., 2021) | al., 2022) | al., 2013) |

| Formatada | |
|------------------|---------------|
| Formatou | |
| Formatada | |
| Tabela Formatada | |
| Formatou | () |
| Formatada | () |
| Formatada | |
| Formatada | |
| Formatada | |
| Formatada | |
| Formatou | |
| Formatou | |
| Formatou | |
| Formatada | |
| Formatada | |
| Tabela Formatada | |
| Formatou | |
| Formatou | () |
| Formatou | |
| Formatada | |
| Formatada | |
| Formatada | |
| Formatou | |
| Formatada | () |
| Formatada | |
| Tabela Formatada | |
| Formatou | |
| Formatou | |
| Formatou | |
| Formatada | |
| Formatada | |
| Formatou | () |
| Formatada | () |
| Tabela Formatada | |
| Formatou | |
| Formatou | |
| | $\overline{}$ |

Formatou Formatou

129 130

131

132

133

134

135

136

137

138

139

140

141

Figure 1: Geographical location of the six study sites across Europe: (a) Värriö, Finland (FI-Var),(b) Hyytiälä, Finland (FI-Hyy), (c) Brasschaat, Belgium (BE-Bra), (d) Fontainebleau-Barbeau, France (FR-Fon), (e) Bosco-Fontana, Italy (IT-BFt) and (f) Castelporziano 2, Italy (IT-Cp2). All photos were retrieved from the ICOS website (https://www.icos-cp.eu/, last access: 20 September 2024)

2.2 Meteorological, Ozone, and Ecosystem Flux Datasets

For each site, the following meteorological variables were available on the ICOS data portal: air temperature (TA, °C), relative humidity (RH, %), short-wave radiation (SW, Wm⁻²), precipitation (P, mm), atmospheric pressure (PA, kPa) and vapour pressure deficit (VPD, hPakPa). Measured half-hourly O₃ concentration data (ppb, Fig. 2) were provided by site principal investigators. The half-hourly Gross Primary Production data (GPP, µmol m⁻²s⁻¹)⁻²s⁻¹) and Latent Heat flux (LE, W m⁻²)⁻²) were derived from eddy covariance measurements at each site. GPP was estimated for the from net ecosystem from net carbon flux measurements acquired by an eddy covariance system exchange (NEE) using standard partitioning techniques implemented in each site the ICOS ONEFlux processing pipeline (Warm Winter 2020 Team, ICOS Ecosystem Thematic

Formatada: Cabecalho

Formatou: Tipo de letra: 9 pt, Negrito, Cor do tipo de letra: Preto

Formatada: Espaço Depois: 10 pt, Espaçamento entre linhas: simples, Limite: Superior: (Sem limites), Inferior: (Sem limites), À direita: (Sem limites), Entre : (Sem limites)

Centre, 2022). LE was derived from water vapour fluxes measured by the same system. All meteorological-data, GPP, and LE₇ data are freelypublicly available onvia the ICOS data portal. The data are infollow the standard format used for theof ICOS L2 ecosystem. The products and are fully compatible with FLUXNET2015. Data processing has been donewas performed using the ONEFlux processing pipeline (https://github.com/icos-etc/ONEFlux) and is fully compliant and integrable with the FLUXNET2015 release (https://fluxnet.fluxdata.org/). pipeline (https://github.com/icos-etc/ONEFlux). Basic site-level statistics and the data extentcoverage are reported in Table 1.

Formatada: Cabeçalho

Formatou: Tipo de letra: 10 pt, Não Negrito, Cor do tipo de letra: Automática



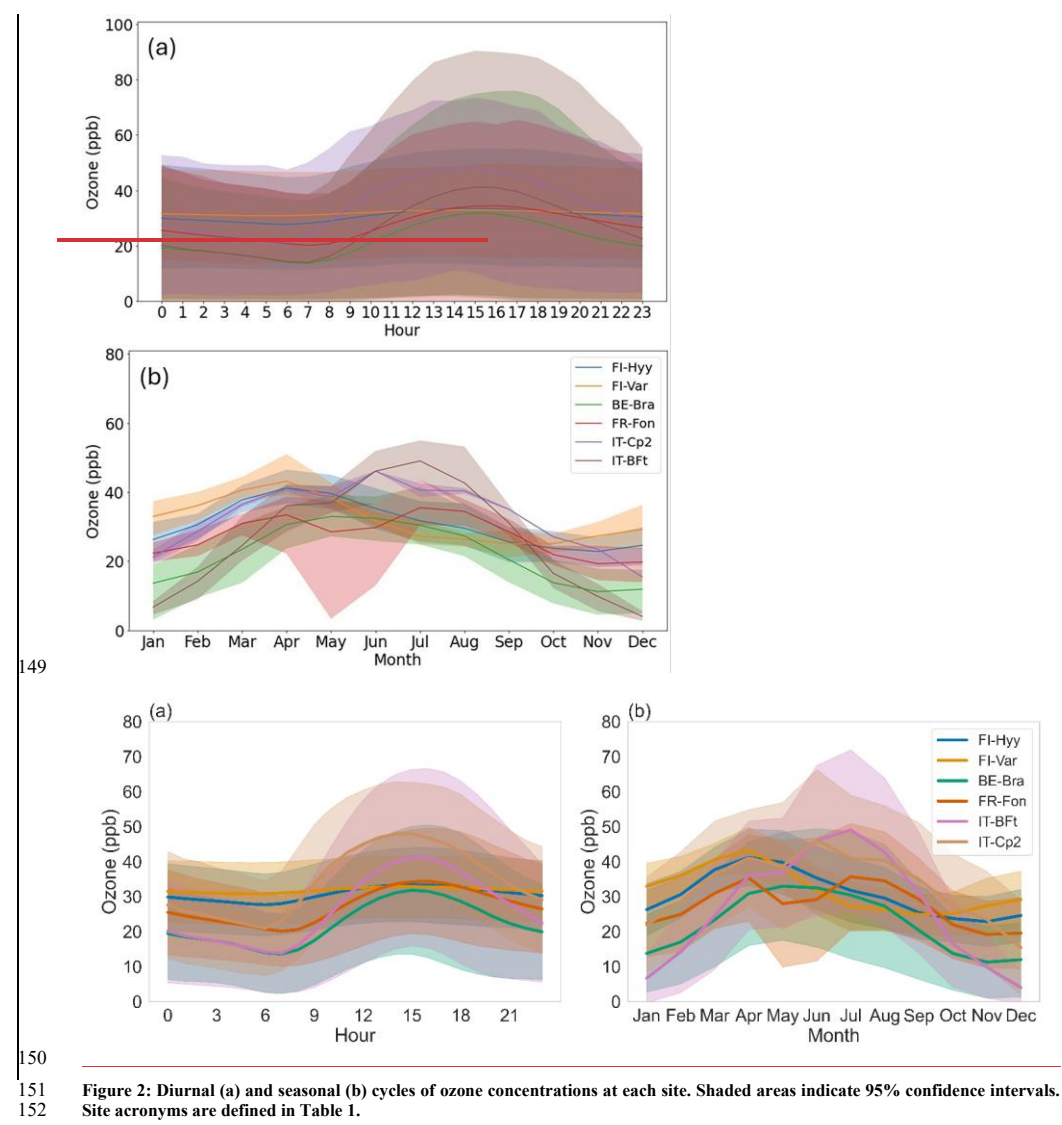


Figure 2: Diurnal (a) and seasonal (b) cycles of ozone concentrations at each site. Shaded areas indicate 95% confidence intervals. Site acronyms are defined in Table 1.

2.3 Statistical analysis: partial correlations

To investigate the specific impact of O₃ on GPP, we used a partial correlation analysis, which measures the strength of a relationship between two variables while controlling for the effect of one or more other variables. This analysis isolates the effects of O₃ on GPP, independent of key environmental drivers such as air temperature, short-wave radiation, and vapour pressure deficit (VPD). Despite this control, subsetting the dataset remains valuable for examining the residual impacts of O₃ under specific environmental conditions. These subsets—summer months and midday hours—represent periods of peak biological activity and photochemical reactions, and, therefore, potential O₃ damage. For example, during the summer, ozone concentrations and GPP are generally higher, while during midday, radiation and photosynthesis peak, likely increasing O₃ uptake through stomata. Subsetting, therefore, helps reveal context-specific dynamics and whether the impacts of O₃ are amplified under these conditions. We used the Python package *Pingouin* (Vallat, 2018) to perform the partial correlations and compute the correlation coefficients and their corresponding significance levels (p-values). All partial correlations were computed using only the observed flux and meteorological datasets, independent of the model simulations. To assess the relationship between GPP and O₃, partial correlations were computed under four configurations for each site:

- 1) Using the entire dataset across all seasons.
- 2) Use summer months only (June, July, and August) when O3 levels are elevated and foliage is fully developed.
- 3) Restricting the analysis to the period between 12:00 and 16:00, coinciding with peak radiation, photosynthesis, and O_3 levels.
- 4) Combining conditions (2) and (3), focusing on summer midday data.

2.4 JULES land surface model

This study utilises JULES version 7.4, a community land surface model widely applied as both a standalone model and the land surface component of the Met Office Unified Model (https://jules.jchmr.org/, last access: 14 July 2024). We employed the offline version of JULES, where we incorporated prescribing in situ observed meteorological, CO_2CO_2 and O_2O_3 datasets as external forcing inputs. Detailed descriptions of JULES can be found in Best et al. (2011), Clark et al. (2011), and Harper et al. (2016). The Farquhar photosynthesis scheme (Farquhar et al., 1980), as implemented by Oliver et al. (2022), models the leaf-level biochemistry of photosynthesis (A, kg C m⁻² s⁻¹) for C₃ vegetation, while the Medlyn scheme (Medlyn et al., 2011) is used to calculate stomatal conductance (g_p , m s⁻¹). The Medlyn approach optimises the stomatal aperture to balance carbon gain with water loss. The stomatal conductance (g_p , m s⁻¹) is represented as:

$$=1.6RT_l \frac{A}{c_a-c_l}$$
 —(1)

where the factor 1.6 represents accounts for the ratio of diffusivities of H_2O to CO_2 through stomata, converting stomatal conductance for from CO_2 to water vapour, units (g_p) , as required for accurately estimating ozone uptake. R is the universal gas

Formatou: Tipo de letra: Não Itálico

Formatou: Não Superior à linha/ Inferior à linha

constant (J mol⁻¹ K⁻¹), T_1 is the leaf surface temperature (K), and c_a and c_i (both Pa) are the leaf surface and internal CO₂ partial pressures, respectively. In this scheme, c_i is calculated as:

$$c_{i} = c_{a} \times \frac{g_{\pm}}{g_{\pm} + \sqrt{d_{q}}}$$

$$= c_{a} \frac{g_{1}}{g_{1} + \sqrt{d_{q}}} \qquad --(2)$$

where d_q is the specific humidity deficit at the leaf surface (kPa), and g_1 (kPa^{0.5}) represents the sensitivity of g_p to the assimilation rate, which is Plant Functional type Type (PFT) dependent. Photosynthesis and stomatal conductance are modelled to respond to changes in environmental drivers (temperature, VPD, incoming radiation, CO₂ concentration and water availability). The impact of soil moisture availability on stomatal conductance is modelled using a dimensionless soil water stress factor (β , unitless) related to the actual soil water content in each layer ($\Theta_{k}\Theta_{k}$, m³ m⁻³) and the critical water content (Θ_{crit} , m³ m⁻³) and water contents at the wilting point ($\Theta_{wit}\Theta_{will}$, m³ m⁻³) and at which the plant starts to become water stressed (Θ_{upp} , m³ m⁻³)). The Θ_{wilt} and Θ_{crit} are derived from soil matric potentials of -1.5 MPa and -0.033 MPa, respectively (Harper et al., 2021):

$$\beta = \begin{cases} \frac{\theta_{k} - \theta_{wilt,k}}{\theta_{upp,k} - \theta_{wilt,k}} & \theta_{wilt,k} \leq \theta_{k} \leq \theta_{upp,k} \\ 0 & \theta_{k} \leq \theta_{wilt,k} \end{cases}$$

$$\beta = \begin{cases} 1 & \text{if } \theta_{k} \geq \theta_{upp} \\ \frac{\theta_{k} - \theta_{wilt}}{\theta_{upp} - \theta_{wilt}} & \text{if } \theta_{wilt} \leq \theta_{k} < \theta_{upp} \\ 0 & \text{if } \theta_{k} < \theta_{wilt} \end{cases}$$
(3)

 θ_{upp} is a function of θ_{crit} , and p_0 (unitless), a PFT-dependent parameter, a threshold at which the plant starts to experience water stress:

$$\theta_{upp} = \theta_{wilt} + (\theta_{crit} - \theta_{wilt})(1 - p_0)$$
 -(4)

In this study, the soil drought stress factor β is calculated from the model-simulated soil moisture in JULES. This approach ensures internal consistency with the model's soil properties, hydraulic structure, and root zone distribution. Observed soil moisture was not used, even where partially available, due to inconsistent quality, limited depth coverage, and lack of harmonised measurements across sites.

2.4.1 JULES: Ozone damage scheme

- The ozone damage scheme implemented in JULES follows the approach of Sitch et al. (2007), incorporating a damage factor
- 212 (F) to quantify O₃-induced reductions in photosynthesis and stomatal conductance. The modified equations for photosynthesis
- 213 (A_{net}) and stomatal conductance (g_s) under O₃ stress are:

$$A_{net} = AF \tag{5}$$

215 g

210

214

216

218

219

223

228

234

$$=g_pA \times F \tag{5}$$

 $217 ext{ } g_s$

$$=g_p \times F$$
 (6)

- where A and g_p are the photosynthesis and the stomatal conductance without O_3 effects, respectively. The damage factor is
- 220 given by: In JULES, photosynthesis and stomatal conductance are first calculated based on standard environmental inputs (e.g.
- 221 light, temperature, VPD and CO₂), without considering ozone. Ozone damage is then applied as a separate multiplicative
- reduction based on the instantaneous stomatal ozone flux. The damage factor is given by:

$$F = 1 - a \times max[F_{03} - F03_{crit}, 0] \tag{7}$$

- where F_{O3} is the O₃ deposition flux through stomata (mmolnmol m⁻² s⁻¹), F_{O3crit} is the threshold for stomatal O₃ uptake (nmol
- 225 m⁻² s⁻¹), and 'a' is the gradient of the O₃ dose-response function (nmol⁻¹ m² s). Both 'a'q and FO3_{crit} are plant functional type
- 226 (PFT) specific parameters. (Table 2). The parameter 'a'a determines the slope of the ozone dose-response function and
- 227 represents how sensitive photosynthesis and stomatal conductance are to O₃ uptake. In JULES, 'a'a has two default values for
 - each PFT, corresponding to "high" and "low" sensitivities to ozone. These two values allow for the exploration of variability
- 229 in plant responses to ozone stress, providing a range of potential outcomes. The flux of O₃ to the stomata (F_{O3}) is modelled
 - in plant responses to ozone stress, providing a range of potential outcomes. The flux of O₃ to the stomata (1 ₀₃) is more
- 230 using a flux gradient approach:

231
$$F_{O3} = \frac{[O_3]}{r_a + \frac{K_{O3}}{g_s}}$$
 (8)

- where $[O_3]$ is the molar concentration of O_3 above the canopy (nmol m⁻³), r_a is the aerodynamic and boundary layer resistance
- 233 (s m⁻¹) and $k_{O3} = 1.67$ (dimensionless) accounts for the relative difference in diffusivities of O_3 and H_2O through leaf stomata.

2.4.2 Calibration of JULES with and without ozone

- 235 In this study, we applied an optimisation approach to calibrate the photosynthesis and stomatal conductance modules in JULES
- 236 for each site using flux tower datasets. This calibration was performed at a half-hourly resolution, ensuring the optimisation
- 237 captures short-term variability in GPP responses to environmental drivers. We focused on the summer months (June to August)
- when O₃ concentrations are typically higher (Table 1, Figure 2), leaves are fully developed, and phenological effects that
- 239 strongly influence seasonal GPP trends are minimised. At each site, 70% of the available GPP and meteorological data were
- 240 randomly selected for model calibration, with the remaining 30% reserved for independent validation. This random sampling.

was applied across the observational period (see Table 1), ensuring both subsets captured a representative range of seasonal and interannual variability.

Optimisation approach

We employed a two-step calibration approach, conducting separate simulations with and without \$\text{O}_{2}\$ effects. We employed_used the Limited-memory Broyden-Fletcher-Goldfarb-Shanno with bound constraints (L-BFGS-B) algorithm, algorithm, which uses dense Hessian approximations and is memory intensive, L-BFGS-B employs a limited memory approach, reducing computational complexity by approximating the Hessian matrix with using a subset of vectors past gradients. This efficiency makes L-BFGS-Bit particularly suitable for optimising a large number of parameters, as required in this study, under bound constraints. The objective function for L-BFGS-B was the Root Mean Square Error (RMSE) between the observed and modelled GPP. Optimisation was implemented in Python using the scipy optimize minimize interface and coupled to JULES via scripted automation. Simulations were monitored using cylc scan to ensure successful completion. Convergence was defined as either an RMSE change < 1×10-10 or a maximum of 1000 iterations. Initial values, By minimising RMSE, we aimed to reduce discrepancies between model predictions and observations, thereby improving the model's predictive accuracy, were drawn from JULES defaults (Table 2), and parameter-specific lower and upper bounds were defined based on plausible biophysical ranges (Table S1). The full list of optimised parameters and their boundaries is provided in Table S1. All parameter trajectories, RMSE values, and convergence diagnostics were robustly logged. A safeguard mechanism was included to prevent runaway iteration or crashes due to I/O interruptions.

Step 1: Optimisation without O3 effects

For the simulations without O₃, we optimised a total of five physiological parameters related to stomatal conductance, photosynthesis, and plant water stress response (Table 2):

- g₁: a parameter related to the stomatal conductance model, which determines the sensitivity of stomatal conductance to the assimilation rate.
- 2. Three photosynthetic parameters:
 - J_{max}: V_{cmax}: the ratio of the maximum potential electron transport rate at 25°C (J_{max}) to Rubisco's maximum rate of carboxylation at 25°C (V_{cmax}).
 - i_v and s_v : the intercept and slope of the linear relationship between Vc_{max} and N_a , the leaf nitrogen per unit area: V_{max}

$$\frac{V_{cmax}}{=i_v + s_v N_a} \tag{7}$$

where N_a Where N_a is calculated as the product of the Leaf mass per unit area and the top-leaf nitrogen concentration.

Formatada: Avanço: Esquerda: 2,54 cm, Sem marcas nem numeração

3. p₀: a parameter describing the plant transpiration response to soil moisture, representing the threshold at which the plant begins to experience drought stress.

Step 2: Optimisation with O₃ effects

275

276

277 278

279

280

281

282

283

284

285

286

287

288

289

290

291

292

293

294

295

296

297

298

299

For simulations with O₃, we extended the optimisation to include two additional ozone-specific parameters:

- FO3_{crit}: the critical flux of O₃ to vegetation, —representing the threshold above which O₃ begins to damage photosynthesis and stomatal conductance.
- 2. μ : an empirical PFT-specific O₃ sensitivity parameter that determines the slope of the O₃ dose-response function.

The optimisation process for simulations with O3 involved two steps:

- Initial optimisation: The same five physiological parameters as in the no-O₃ simulations were optimised, along with FFO3_{crit} and α.
- 2. Local refinement: To further improve model accuracy under O₃ stress conditions, we performed a local refinement of FO3_{crit} and \(\rho\). Using the optimised parameter set from the initial step, we systematically explored a fine grid of values around the best-performing FO3_{crit} and a. Step sizes ranging from 0.005 to 0.025 were used to refine the parameter estimates. Model performance was evaluated for each simulation using RMSE, and the best parameter set was selected based on its agreement with observed half-hourly GPP values.

Model configurations

In total, we considered two types of simulations (Figure 3):

- 1. Default simulations: Site level runs using four model configurations (Table 3): default model parameters (Oliver et al., 2022; Harper et al., 2016; Harper et al., 2021), with and without Os effects.
- 2. Optimised simulations: Site-level runs using optimised parameters, simulations, each with and without O3 effects.

ozone. For each site, this setup enabled a direct comparison of model skill under default and optimised simulations without O₃, parameter sets, as well as the ealibrated parameters included g₁, J_{max}: V_{emax}, i₂, s₃, and p₀. For optimised simulations with O₃, we additionally ealibrated FO₃ entrand amechanistic contribution of ozone effects.

Table 2: Default parameter values of the JULES for each site.

| Parameter | Name | Unit | FI-Hyy | FI-Var | BE-Bra | FR-Fon | IT-BFt | IT-Cp2 |
|----------------|---|--------|--------|--------|--------|--------|--------|--------|
| g ₁ | Sensitivity | kPa0.5 | 2.35 | 2.35 | 2.35 | 4.45 | 4.45 | 3.37 |
| | of the stomatal conductance to the | | | | | | | |

Formatou: Tipo de letra: Itálico

Formatada: Cabecalho

Formatou: Tipo de letra: Itálico

Formatou: Tipo de letra: Itálico

Formatada: Esquerda

Formatou: Inferior à linha

Formatou: Tipo de letra: 10 pt

Formatou: Tipo de letra: 10 pt

Formatou: Tipo de letra: 10 pt, Não Superior à linha/

Inferior à linha

Formatou: Tipo de letra: 11 pt

Formatou: Tipo de letra: 10 pt

Formatou: Tipo de letra: 11 pt

Formatou: Tipo de letra: 10 pt

Formatou: Tipo de letra: 11 pt

Formatou: Tipo de letra: 10 pt

Formatou: Tipo de letra: 11 pt

Formatou: Tipo de letra: 10 pt

Formatou: Tipo de letra: 11 pt

Formatou: Tipo de letra: 10 pt

Formatou: Tipo de letra: 11 pt

Formatou: Tipo de letra: 10 pt

Formatou: Tipo de letra: 11 pt

Formatada: Espaçamento entre linhas: simples

Formatada: Esquerda

| | assimilatio | n | | | | | | | |
|-----------------------------------|--------------------|-------------------|-------|-------|-------|-------|-------|-------|----------|
| | rate | | | | | | | | |
| J _{max} :V _{cm} | Ratio of | Ā | 1.48 | 1.48 | 1.48 | 1.78 | 1.78 | 1.63 | |
| ax | Jmax to | | | | | | | | |
| | Vcmax | | | | | | | | |
| | at 25 | | | | | | | | |
| | deg C | | | | | | | | |
| i_v | Intercept of | | 6.32 | 6.32 | 6.32 | 5.73 | 5.73 | 3.90 | |
| | the linear | CO2, m-2, | | | | | | | |
| | relationship | s-1 | | | | | | | |
| | between | | | | | | | | |
| | Vcmax and | | | | | | | | |
| | Na | | | | | | | | |
| $\mathbf{S}_{\mathbf{v}}$ | Slope of | μmol | 18.15 | 18.15 | 18.15 | 29.81 | 29.81 | 28.40 | |
| | the | CO2 gN- | | | | | | | |
| | linear | 1 s-1 | | | | | | | |
| | relation | | | | | | | | |
| | ship | | | | | | | | |
| | between | | | | | | | | |
| | Vcmax | | | | | | | | |
| | and Na | | | | | | | 1 | <u> </u> |
| $\mathbf{p_0}$ | threshold | Ā | 0 | 0 | 0 | 0 | 0 | 0 | |
| | at which | | | | | | | | |
| | the plant | | | | | | | | |
| | starts to | | | | | | | | |
| | experience | | | | | | | | |
| | water | | | | | | | | |
| | stress | | | | | | | | |
| FO3 _{crit} | Critical | - A | 1.6 | 1.6 | 1.6 | 1.6 | 1.6 | 1.6 | |
| | flux of | 2 _s -1 | | | | | | | |
| | 03 to | | | | | | | | |
| | vegetati | | | | | | | | |
| # | on | | 0.055 | 0.055 | 0.055 | 0.45 | 0.45 | 1015 | |
| "High" | PFT- | nmol-1 | 0.075 | 0.075 | 0.075 | 0.15 | 0.15 | 0.15 | |
| a | specific 03 | m2.s | | | | | | | |
| | sensitivity | | | | | | | | |
| "T" | parameter | 1.4 | 0.02 | 0.02 | 0.02 | 0.04 | 0.04 | 0.04 | |
| "Low" | PFT- | nmol-1 | 0.02 | 0.02 | 0.02 | 0.04 | 0.04 | 0.04 | |
| a | <u>specific</u> | <u>m2 s</u> | | | | | | | |
| | <u>03</u> | | | | | | | | |
| | <u>sensitivity</u> | | | | | | | | |
| | parameter | | | | | | | | |

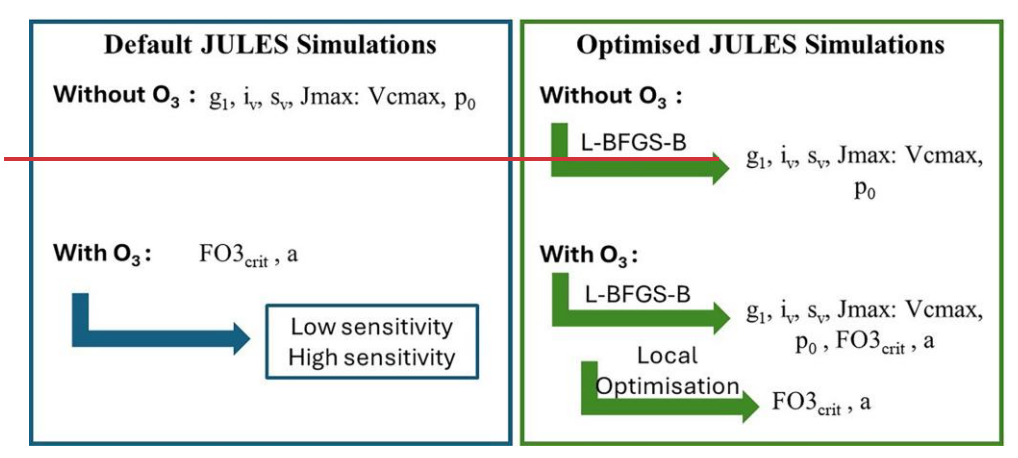
| Formatada | |
|------------------|----|
| Formatou | [] |
| Formatou | |
| Formatada | |
| Formatada | |
| Tabela Formatada | [) |
| Formatou | |
| Formatou | |
| Formatou | |
| Formatada |) |
| Formatou | |
| Formatou | |
| Formatou | |
| Formatou | |
| Formatou | [] |
| Formatou | |
| | |

Formatada

Tabela Formatada

Formatou

Formatou Formatada Formatou



FigureTable 3: Overview of the two types of simulations considered in this study. Default simulations represent site-level runs with model default parameters with or without O3 effects. Simulations with optimised parameters are also run with and without O3 effects. ForIn the optimised simulations without ozone, thefive parameters were calibrated—are: the sensitivity of stomatal conductance to the assimilation rate (g1), the intercept (iv) and the slope (sv) of the linear relationship between V_{cmax} and Na, the ratio between the carboxylation rate and the rate of electron transport at 25°C (J_{max}:V_{cmax}) and the threshold at which the plant starts to experience drought stress (p0). For configurations with O3, we also add the critical flux of O3 to vegetation (Fo3crit) and PFT-specific O3 sensitivity parameter (a).

| Configuration | O ₃ effects | Optimised parameters |
|----------------------------------|------------------------|--|
| Default (no O ₃) | <u>No</u> | <u>None</u> |
| Default (with 0 ₃) | <u>Yes</u> | <u>None</u> |
| Optimised (no O ₃) | <u>No</u> | g ₁ , I _{max} : V _{cmax} , i _v , S _v , p ₀ |
| Optimised (with O ₃) | Yes | g ₁ , I _{max} ; V _{cmax} , i _v , s _v , p ₀ , FO3 _{crit} , a |

Model evaluation

In order to evaluate the model performance, JULES was forced with the meteorology, CO_2 and O_3 observed at each site and evaluated against flux GPP data. In all simulations, the vegetation cover was prescribed using JULES default PFTs. -In each simulation, phenology was simulated prognostically, allowing the model to simulate the dynamic evolution of the maximum leaf area index (LAI). Prior to running the simulations, the model underwent a 50-year spin-up phase to ensure that the model state variables were representative of steady-state conditions. We used Root Mean Squared Error (RMSE) and the coefficient of determination (r^2) to quantify the differences between the outputs from the various model simulations and the observations.

2.4.3 High-O₃ days analysis

To investigate the impact of elevated ozone concentrations on diurnal GPP dynamics and their interaction with latent heat (LE) and vapour pressure deficit (VPD), we analysed the temporal patterns of these variables on the days O₃ concentration is above 40 ppb for each site. Additionally, the performance of different model configurations was evaluated for these specific high-ozone days to assess their ability to capture observed GPP responses under extreme conditions.

To address our third research question—how ozone impacts interact with other environmental factors and how an optimised model can help elucidate these mechanisms—we focused on days when ambient ozone concentrations exceeded 40 ppb at each site. These high-ozone events typically coincide with elevated solar radiation and vapour pressure deficit (VPD), which can enhance stomatal ozone uptake and intensify physiological stress. For each site, we analysed the diurnal cycles of observed GPP, modelled GPP with and without ozone effects, as well as modelled stomatal conductance, latent heat flux (LE), VPD, the soil moisture stress factor (β), and ozone flux to vegetation (FO₃). The flux FO₃ represents the actual rate of ozone uptake through stomata, computed in JULES from canopy-level ozone concentrations and stomatal plus aerodynamic resistances. The variable β is a dimensionless scaling factor (ranging from 0 to 1) that modulates stomatal conductance in response to soil moisture availability. It reflects the degree of physiological drought stress as perceived by the plant and is derived from the soil water content and site-specific hydraulic thresholds (e.g. wilting point, p₀). We used β instead of raw plant-available soil moisture because it is directly integrated into the stomatal conductance formulation in JULES, ensuring model-consistent representation of water stress. Unlike absolute soil moisture, which varies with soil texture and rooting depth, β normalises water limitation in a physiologically meaningful and site-comparable way. This diagnostic framework enabled us to evaluate how well the optimised model captures dynamic interactions between ozone exposure and environmental stressors during high-risk periods. We compared observed and simulated GPP responses across different environmental regimes and examined site-specific optimised parameters, including g₁, p₀, a, and FO3_{crit}. Our aim was to determine whether GPP reductions are primarily driven by (a) stomatal limitation due to drought and/or high VPD, (b) biochemical ozone damage due to high cumulative ozone uptake, or (c) the simultaneous presence of multiple environmental stressors.

The inclusion of modelled stomatal conductance and FO_3 allows direct tracing of ozone uptake, while the soil moisture stress factor β provides a mechanistic indicator of water limitation. This approach supports a process-level understanding of the mechanisms underlying ozone impacts on carbon uptake during extreme conditions.

2.4.34 GPP reductions due to ozone

320

321

322

323

324

325

326

327

328

329

330

331

332

333

334

335

336

337

338

339

340

341

342

343

344

345

346

347

348

349

350

To quantify the overall impact of Θ_2O_3 on GPP, we calculated the relative reduction in GPP for each site using the optimised simulations and the configuration without O_3 impact as the baseline. This calculation was performed each year to account for interannual variability, and the results were averaged to obtain the mean relative reduction over the study period. We define forest sensitivity to O_3 as the percentage reduction in mean annual GPP between the optimised simulations with and without ozone effects. Additionally, we use partial correlation coefficients between observed GPP and ozone concentrations, while

controlling for temperature, radiation, and vapour pressure deficit, as a complementary indicator of site-level sensitivity or resilience. Together, these metrics provide a consistent, quantitative framework for classifying sites as either ozone-sensitive or ozone-resilient and are applied throughout the manuscript in both model evaluation and the interpretation of site-specific responses.

3 Results

351

352

353

354

355

356

357

358

359

360

361

362

363

364

365

366

367

368

369

370

371

372

373

374

375

376377

378

379

380

381

3.1 Statistical Analysis: Partial correlations

The results of the partial correlation analysis highlight varying degrees of GPP sensitivity to ozone across the investigated sites (Fig. 43), Hyytiälä (FI-Hyy), Värriö (FI-Var), Brasschaat (BE-Bra), Fontainebleau-Barbeau (FR-Fon), and Bosco-Fontana (IT-BFt) exhibited consistently negative correlations between GPP and O₃, indicating a significant vulnerability to ozone pollution. The negative impact of ozone on GPP is particularly pronounced during specific conditions, such as the summer months (June, July, and August) and midday hours when radiation and temperature are high. While partial correlations control for key environmental variables such as temperature, radiation, and VPD, subsetting the dataset allows for an investigation of the residual impacts of O3 under specific ecological conditions. These subsets, such as summer months or midday hours, represent periods of peak biological activity and potential O₃ damage, making them ecologically and practically relevant. For instance, ozone O₃ concentrations and GPP are generally higher tend to peak during the summer due to enhanced photochemical production from increased solar radiation, higher temperatures, and elevated emissions of ozone precursors (NO_x and VOCs). While plant activity contributes to biogenic VOC emissions, it also increases ozone deposition via stomatal uptake, leading to complex and site-dependent seasonal patterns. Subsetting ensures the analysis captures O₃ impacts under these seasonal conditions. Similarly, during midday hours, when radiation and photosynthesis peak, O3 uptake through stomata may also reach its highest levels. This approach allows us to determine whether O3 impacts are consistent across varying contexts or are amplified under specific conditions of heightened environmental and biological activity. Across the sites, FI-Hyy showed weak but significant negative correlations across all subsets, indicating a mild sensitivity to ozone. FI-Var exhibited slightly stronger negative correlations than FI-Hyy, particularly during midday hours in the summer, emphasising the vulnerability of boreal forest ecosystems to ozone stress under specific conditions. BE-Bra and IT-BFt demonstrated the most pronounced negative correlations during the combined summer and midday subsets, suggesting that these conditions heighten the vulnerability of these sites to ozone pollution. Notably, BE-Bra showed the strongest correlation during the summer midday period, underscoring the importance of environmental stressors in exacerbating ozone effects. FR-Fon also displayed significant negative correlations, although the magnitude was generally lower than at BE-Bra and IT-BFt, indicating a moderate sensitivity to ozone.

Formatada: Espaço Depois: 6 pt

Conversely, the Castelporziano 2 (IT-Cp2) site exhibitedshowed a negative correlation when considering using the full dataset;

however, correlations for other subsets, the correlation coefficients subset periods became positive and non-significant. This

ific site

Formatada: Cabeçalho

outcome may stem frombe due to the limited dataset available data availability for IT-Cp2 and the unique specific site characteristics of this site, including, such as partial stomatal closure in response to drought and high VPD-stress during warm seasons. These factors may obscure the direct relationship between ozone and GPP at this Mediterranean site.

Overall, the results emphasise the varying impacts of ozone across different environmental contexts and site-specific.

Overall, the results emphasise the varying impacts of ozone across different environmental contexts and site-specifical conditions. Subsetting the data to account for periods of peak biological activity enhances our understanding of the residual effects of O₃ on GPP after controlling for other critical environmental variables. This nuanced approach provides offers valuable insights into the dynamics of ozone stress across diversevarious European forest ecosystems in Europe.

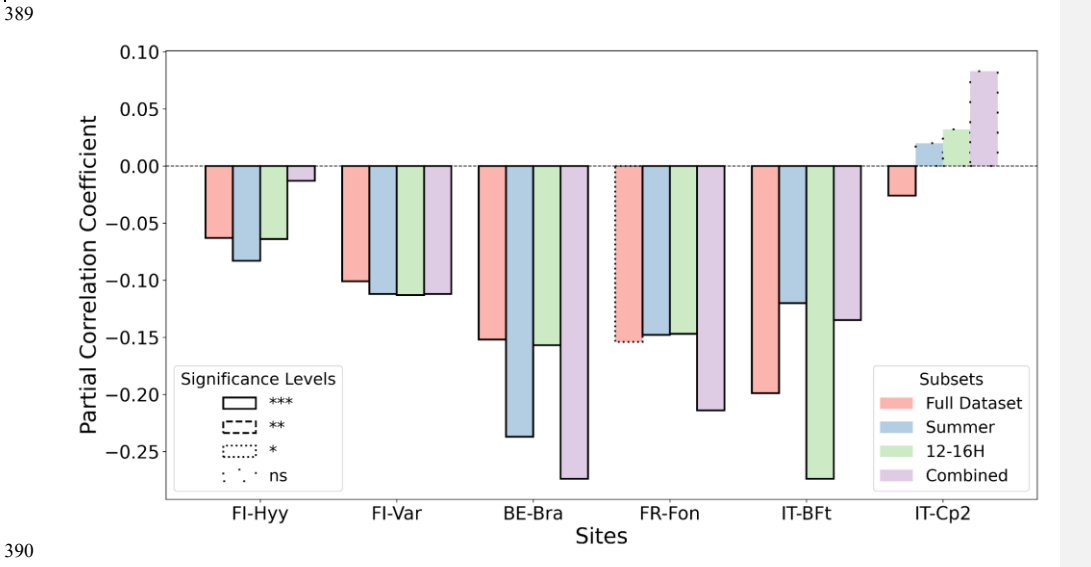


Figure 43: Partial correlation coefficients (unitless) between GPP and O_3 – after controlling for air temperature, short-wave radiation and vapour pressure deficit. The calculations were performed for all datasets (salmon bars), including summer only (blue bars, June, July, and August), midday only (green bars, 12-16H), and midday summer only (purple bars, combined). The significance levels: p-value < 0.001 ***, p-value < 0.01 **, p-value < 0.05 *, non-significant (ns).

3.2 JULES GPP simulations

The default JULES model configuration (default parameters, Table 34 and Fig. 54) generally exhibits higher variability and larger deviations from observed GPP values across all sites. The optimisation significantly improves model performance by reducing RMSE and increasing r² values across most sites (Table 34). However, the incorporation of O₃ effects yields mixed results, with improvements in RMSE at certain sites (e.g., FR-Fon, IT-BFt) but little to no improvement at others, such as FI-Hyy and BE-Bra (Table 34).

Formatada: Espaço Antes: 0 pt, Depois: 0 pt

Formatada: Espaço Depois: 0 pt

At FI-Hyy, both default and optimised models perform well, with slight improvements in RMSE and r^2 following optimisation. The optimised simulation with O₃ achieves the greatest reduction in RMSE (2.11 μ mol CO₂ m⁻² s⁻¹), a 27% decrease relative to the optimised no O₃ case (2.88 μ mol CO₂ m⁻² s⁻¹), and an increase in r^2 (to 0.86)- (+3.6%). These improvements reflect the model's ability to adjust to local conditions with minimal parameter changes (Fig. 6), particularly in boreal settings. However, the inclusion of O₃ does not significantly alter RMSE, suggesting that GPP at this site is not highly sensitive to ozone stress. This limited impact is consistent with the relatively low ambient ozone concentrations observed at FI-Hyy, which reduce the

potential for strong O₃-induced reductions in GPP.

At FI-Var, optimisation reduces underestimations during midday peaks and aligns simulated GPP with observations. Therefore, the optimised configuration achieves a 1.65 μmol CO₂ m⁻² s⁻¹ RMSE (<u>-32% relative to 2.41</u>) and <u>a r² value of 0.75 r².(±2.7%).</u> Key parameter adjustments, such as increases in g₁ and decreases in p₀ (Figs. 6a5a and 6e5c), contribute to these improvements. Incorporation of O₃ effects only slightly improves RMSE at FI-Var, suggesting moderate sensitivity to ozone impacts at this boreal site.

At BE-Bra, the default configuration performs well, and optimisation further reduces RMSE and improves r^2 . The optimised simulation achieves an RMSE of 3.36 μ mol CO₂ m^{-2} s^{-1} (-14.3% from 3.92) and an r^2 of 0.81; (+5.2% from 0.77), highlighting the importance of fine-tuning parameters such as g1 and sy (Figs. 6a5a and 6d5d). However, the inclusion of O₃ has a minimal impact on RMSE at this site, suggesting relatively low ozone sensitivity compared to other locations.

At FR-Fon, default simulations significantly underestimate GPP during peak hours, especially under high ozone stress. The optimisation improves model accuracy, showing a reduction in RMSE (5.71 µmol CO₂ m⁻² s⁻¹)⁻¹, -35% from 8.72) and an increase in r² (0.60, +22.4% from 0.49). Despite these improvements, some underestimation remains, indicating that additional refinement of O₃ response mechanisms or GPP modelling may be needed at this site.

At IT-BFt, the default model exhibits large variability in GPP, reflecting the challenges of modeling Mediterranean ecosystems. The optimised configuration achieves the greatest improvements, reducing RMSE to 3.78 µmol CO₂ m⁻² s⁻¹ (-13.1% from 4.35) and increasing r² to 0.82-(+9.3% from 0.75). Adjustments toof FO3crit, a, and p0 (Fig. 6f, 6g5f, 5g, and 6e5c) enhance performance by addressing both accounting for the combined effects of ozone and water stress, highlighting the strong impact of O-which act as co-limiting factors during the summer and jointly contribute to reduced GPP at this site.

At IT-Cp2, the default model underestimates GPP during midday peaks, particularly under ozone stress. The optimised configuration achieves the best results, reducing RMSE to 2.85 µmol CO₂ m⁻² s⁻¹ (-22.8% from 3.69) and increasing r² to 0.72- (+2.9% from 0.70). Adjustments to FO3crit and a play a critical role in capturing ozone impacts at this Mediterranean site, demonstrating the necessity of refining these parameters in high-ozone environments.

Overall, parameter optimisation improves model accuracy and reliability across all sites. However, the inclusion of O₃ effects leads to site-specific responses, with improvements in RMSE at some sites (e.g., FR-Fon, IT-BFt) but minimal changes in r² across most locations. Figure 54 highlights that in some cases, the addition of O₃ increases imulations including O₃ effects exhibit increased model biases, despite RMSE values suggesting only slight degradation in performance. These findings

Formatada: Cabeçalho

Formatada: Espaço Depois: 0 pt

Formatou: Não Superior à linha/ Inferior à linha

Formatou: Não Superior à linha/ Inferior à linha

Formatada: Espaço Depois: 0 pt

Formatou: Não Superior à linha/ Inferior à linha

Formatou: Tipo de letra: Não Itálico

Formatou: Não Superior à linha/ Inferior à linha

Formatada: Espaço Depois: 0 pt

Formatou: Não Superior à linha/ Inferior à linha

Formatou: Tipo de letra: Não Itálico

underscore the need for continued refinement of ozone response mechanisms to improve model accuracy, particularly in Mediterranean regions where ozone exposure and water stress are strongly coupled.

434

435

436

437

438

Table $\frac{34}{2}$: Summary of model evaluation metrics: root mean square error (RMSE, μ mol CO₂ m⁻² s⁻¹) and coefficient of determination (r²) values for each site. The metrics are calculated for default and optimised simulations with and without ozone impacts.

| | FI- | FI- | FI- | FI- | BE- | BE- | FR- | FR- | IT- | IT- | IT- | IT- | 4 |
|------------------------|------|----------------|------|----------------|-------------|----------------|-------------|----------------|-------------|----------------|-------------|----------------|---|
| | Hyy | Hyy | Var | <u>Var</u> | Bra | <u>Bra</u> | Fon | <u>Fon</u> | BFt | <u>BFt</u> | Cp2 | <u>Cp2</u> | Γ |
| Default | | | | | | | | | | | | | 4 |
| Metrics | RMSE | r^2 | RMSE | \mathbf{r}^2 | RMSE | \mathbf{r}^2 | RMSE | \mathbf{r}^2 | RMSE | \mathbf{r}^2 | RMSE | \mathbf{r}^2 | 4 |
| Without O ₃ | 2.88 | 0.83 | 3.87 | 0.63 | 4.06 | 0.76 | 9.53 | 0.39 | 6.30 | 0.53 | 3.81 | 0.65 | |
| With O ₃ | 2.85 | 0.83 | 3.08 | 0.65 | 3.97 | 0.77 | 8.85 | 0.48 | 5.78 | 0.60 | 3.73 | 0.69 | |
| Optimised | | | | | | | | | | | | | |
| Metrics | RMSE | \mathbf{r}^2 | RMSE | \mathbf{r}^2 | RMSE | \mathbf{r}^2 | RMSE | \mathbf{r}^2 | RMSE | \mathbf{r}^2 | RMSE | \mathbf{r}^2 | 4 |
| Without O ₃ | 2.88 | 0.83 | 2.41 | 0.73 | 3.92 | 0.77 | 8.72 | 0.49 | 4.35 | 0.75 | 3.69 | 0.70 | Ī |
| With O ₃ | 2.11 | 0.86 | 1.65 | 0.75 | 3.36 | 0.81 | 5.71 | 0.60 | 3.78 | 0.82 | 2.85 | 0.72 | 1 |

Formatada Células Inseridas Células Inseridas Células Inseridas Células Inseridas Células Inseridas Células Inseridas Formatou Formatou Formatou Formatou Formatou Formatou Formatada Formatada Formatada Formatada **Formatada** Formatada Células Inseridas Células Inseridas Formatou

Formatada
Células Inseridas
Células Inseridas
Células Inseridas
Formatou
Formatou
Formatou
Formatou
Formatou
Células Inseridas
Células Inseridas
Células Inseridas
Células Inseridas

Células Inseridas Células Inseridas Células Inseridas Células Inseridas



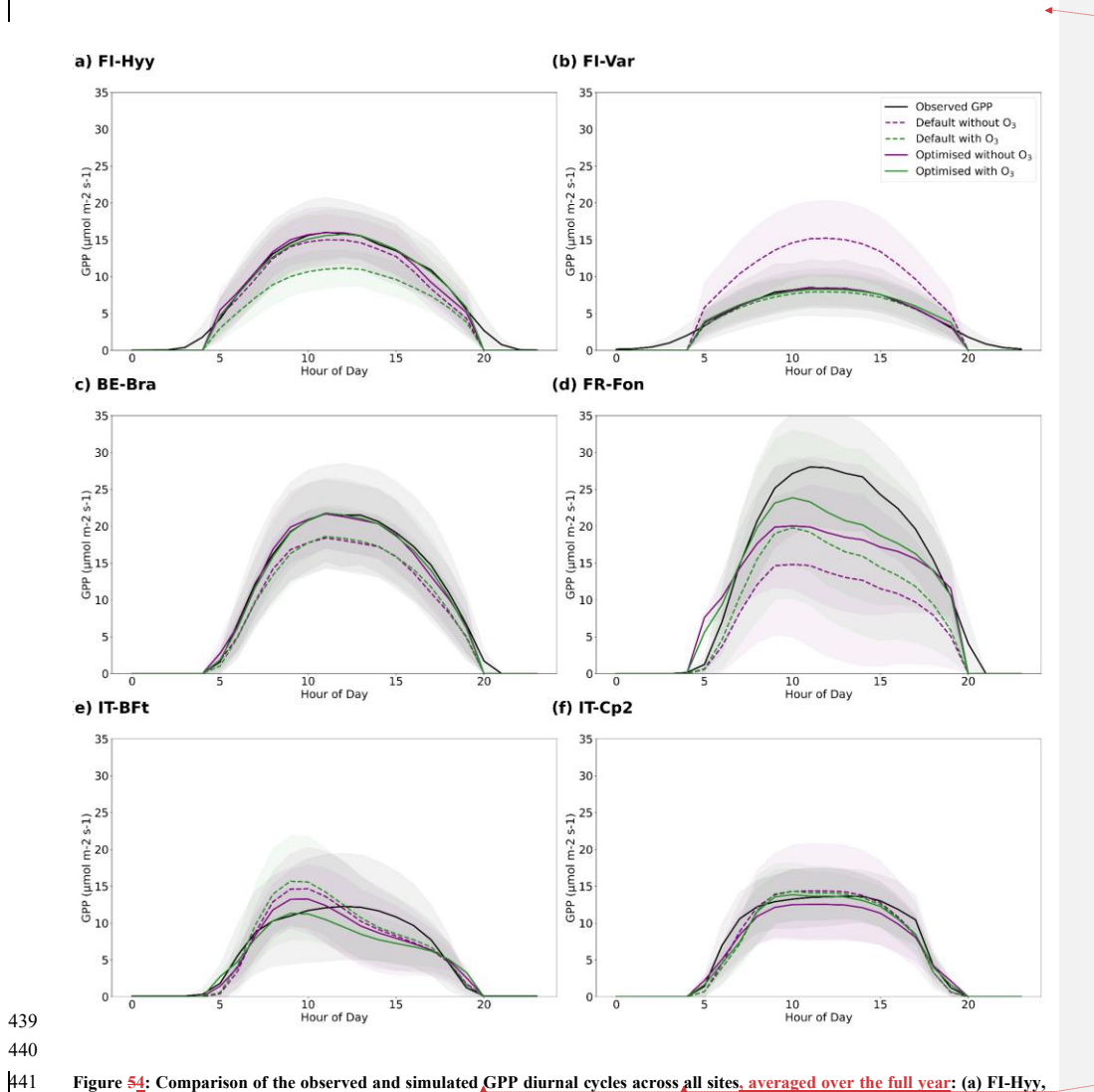


Figure 54: Comparison of the observed and simulated GPP diurnal cycles across all sites, averaged over the full year: (a) FI-Hyy, (b) FI-Var, (c) BE-Bra, (d) FR-Fon, (e) IT-BFt and (f) IT-Cp2. Shaded areas encompass plus and minus one standard deviation. The black line represents the observed GPP. The default simulated GPP are the dashed purple line (without O₃) and dashed green line (with O₃), and optimised simulated GPP are the purple line (without O₃) and green line (with O₃).

442

443

444

Formatou: Cor do tipo de letra: Preto

Formatou: Cor do tipo de letra: Preto



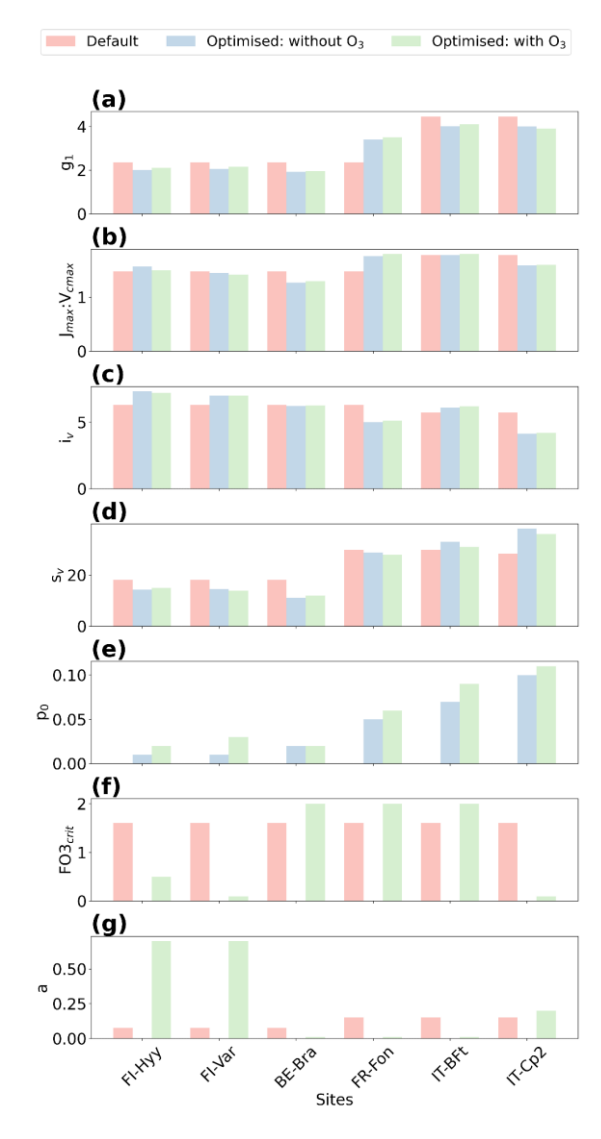


Figure 65: Comparison of default and optimised parameters. The figure presents a comparison between the default (salmon bars) and optimised parameter values: without ozone (blue bars) and with ozone (green bars) for the six sites. The parameters include (a) stomatal conductance sensitivity to assimilation rate (g1), (b) the ratio of maximum potential electron transport rate to maximum carboxylation rate (Jmax! Vcmax), (c) and (d) parameters related to leaf nitrogen (is and ss), (e) soil moisture stress threshold (p0), (f) the critical ozone flux (FO3crit), and (g) the sensitivity parameter (a).

3.3 Interaction of O₃ with environmental factors on GPP during high ozone days

For high O₃ days (above 40 ppb), across all sites, the observed GPP shows a characteristic peak around midday, with simulated GPP that includes Θ_2 effects generally aligning more closely with the observed data compared to simulations that exclude Θ_2 of effects (Fig. 76). However, the magnitude of this improvement varies by site.

Ozone concentrations follow a diurnal cycle, peaking in the afternoon (12:00–16:00) across all sites. This peak reflects the influence of high solar radiation, temperature, and atmospherie boundary layer dynamics-, including the entrainment of ozone-rich free tropospheric air masses that contribute to surface ozone enhancement. The impact of O₃ on GPP is modulated by interactions with key environmental factors such as vapour pressure deficit (VPD) and, latent heat flux (LE), both of which influence and soil moisture stress (β), each influencing stomatal conductance. When (g₃) and thereby ozone uptake (FO₃). LE reflects evaporative demand and water availability, while β provides a direct measure of soil moisture constraint on stomatal opening. FO₃ represents the actual flux of ozone into the leaves via stomata, and g₃ integrates the stomatal response to multiple environmental drivers, including VPD and LE peak aroundsoil water availability. Around midday, when VPD and LE typically peak, stomatal conductance typically increases, facilitating greater O₃ uptake and intensifying may decline as a protective response to water loss. However, the simultaneous increase in radiation and temperature can elevate ambient O₃ concentrations and photosynthetic demand. These competing environmental influences affect O₃ uptake and its effects impact on photosynthesis-, depending on site-specific conditions and plant water regulation strategies.

Formatada: Sem controlo de linhas isoladas, Manter linhas juntas

Formatada: Sem controlo de linhas isoladas

O3 effects. At Figure 6 highlights these dynamics using averaged diurnal cycles of GPP, O3, VPD, LE, gs, FO3, and β during high-O₃ days. At the two boreal sites (FI-Hyy and FI-Var), ozone peaks reach moderate levels (~46 and 44 ppb, respectively), but their impacts on GPP differ (Table 5). FI-Var shows minimal response to ozone, with an RMSE reduction of just 0.9% (from 3.10 to 3.07 µmol CO₂ m⁻²s⁻¹), suggesting low ecological sensitivity. g₈ and FO₃ values remain relatively low throughout the day, and β values are near 1, indicating no significant soil moisture limitations or stomatal downregulation. In contrast, FI-Hyy exhibits a large RMSE improvement, from 9.97 to 0.52 μmol CO₂ m⁻² s⁻¹ (a 94.8% reduction), when ozone effects are included. However, this performance gain does not reflect sustained biological sensitivity. Instead, it stems from a systematic overestimation of GPP by the ozone-free model during high-O₃ episodes. These episodes are rare (see Table 1), but when they do occur, the model without ozone consistently overestimates GPP. The inclusion of ozone damage corrects this bias. The partial correlation analysis, combined with the limited ambient ozone exposure outside these rare events, supports this interpretation. We therefore distinguish between improved model-data agreement due to structural correction and true ecological ozone sensitivity, the latter being more clearly limited at FI-Var. FI-Hyy, however, simulations without O₃ significantly underestimate GPP, leading to a high RMSE (9.97 µmol CO₂ m⁻² s⁻¹), which improves dramatically when O₂ effects are included (RMSE = 0.52 μmol CO₂ m⁻² s⁻¹). This suggests that while FI-Hyy is less sensitive to O₃ overall, proper parameterisation of O₃ effects improves model performance. At BE-Bra, GPP reductions due to ozone are more pronounced, with RMSE dropping from 7.57 to 3.09 umol CO₂ m⁻² s⁻¹ 09 μmol CO₂ m⁻² s⁻¹, a 59.2% improvement when O₃ effects are considered. This improvement highlights the need to include ozone stress in GPP simulations, particularly in temperate forests where stomatal ozone uptake remains substantial. In Figure 6, gs and FO3 both exhibit midday peaks despite elevated VPD, indicating that stomatal conductance is not fully downregulated under higher evaporative demand, thus allowing more ozone to enter the leaf and cause damage. Interestingly, at FR-Fon, while ozone peaks coincide with midday GPP declines, the difference between with and without O3 simulations is small in Figure 7, This is confirmed by the minor RMSE reduction (from 5.60 to 5.47 \text{ \text{ \text{mmol CO}} \text{ \text{m}} = s^-1, Table 4),47 \text{ \text{ \text{mmol CO}} \text{ \text{m}} = s^-1}

At boreal sites (FI-Hyv and FI-Var), ozone peaks reach moderate levels (~46 and 44 ppb, respectively), yet their impact on

GPP appears limited. FI-Var, in particular, shows minimal reductions in GPP, suggesting that this site is relatively resilient to

ozone stress. This is reflected in the small RMSE improvement (3.10 to 1.18 umol CO₂ m⁻² s⁻¹. Table 4) when incorporating

467

468

469

470

471

472

473

474

475

476

477

478

479

480

481

482

483

484

485

486

487

488

489

490

491

492

493

GPP at this site.

Formatou

Formatou

Formatou

Formatou

Formatou

Formatou

Formatou

Formatou

Formatou

(2.3%), suggesting that other factors—, such as phenology or local climate conditions—, play a dominant role in regulating

, and that actual ozone uptake is likely limited despite ambient concentrations. Mediterranean sites (IT-BFt and IT-Cp2) experience the highest ozone peaks (>60 ppb), which coincide with sharper midday declines in GPP. Unlike boreal and temperate sites, where O₃ effects were moderate, these ecosystems exhibit stronger O₃-60 ppb). At IT-BFt, the JULESsimulated GPP exhibits a pronounced midday decline, particularly in the optimised configuration with ozone effects, indicating a strong response to midday ozone stress. In these simulations, g_s shows a clear midday drop, while FO₃ remains high during that period, suggesting that ozone uptake still occurs despite partial stomatal closure. However, the observed GPP shows only a slight morning dip and continues increasing into the afternoon. This divergence points to a potential overestimation of mid day stomatal limitation or ozone effects in the model. At IT-Cp2, no distinct midday depression is observed in either the simulated or partitioned GPP. FO₃ is modest, and β remains close to 1 throughout the day, indicating minimal water stress and limited ozone uptake. While these sites do show noticeable reductions in RMSE after including ozone effects, 0.8% at IT-BFt (from 5.88 to 5.83 µmol CO₂ m⁻² s⁻¹) and 64.6% at IT-Cp2 (from 5.45 to 1.93 µmol CO₂ m⁻² s⁻¹), these improvements are not the largest among all sites. Indeed, FI-Hyy and BE-Bra show greater RMSE reductions during high ozone days. This suggests that while Mediterranean sites face high ozone concentrations, the degree of ozone-induced reductions in GPP. At IT Cp2, including Os in the model reduces RMSE from 5.45 to 1.93 µmol CO2 m⁻² s⁻¹, the most significant improvement across all sites. Similarly, at GPP reduction may vary depending on the interplay of environmental stressors and model representation. The results IT-BFt, RMSE drops from 5.88 to 2.31 µmol CO₂ m⁻² s⁻¹. These reductions highlight the necessity importance, of incorporating Os stress insite-specific calibration and caution against generalising, Mediterranean regions, where high VPD and stomatal conductance increasesites as the most ozone uptake, amplifying physiological stress. -sensitive solely based on ozone concentration levels. Interestingly, despite thealthough JULES simulates strong midday GPP declines in GPP at Mediterranean sites, Figure 6 suggests 5 shows that the ozone sensitivity parameters are generally lower in Mediterranean forests. This indicates that the observed ozone effects in these regions are primarily driven by higher ambient O3 concentrations rather than an inherently higher sensitivity of Mediterranean vegetation for Mediterranean forests. This pattern may reflect the fact that high VPD and limited soil moisture in these regions reduce stomatal conductance during midday, thereby lowering actual ozone uptake and mitigating its physiological effects, despite high ambient O₃ concentrations. This dynamic, documented in several previous studies (Lee et al., 2013), suggests that the observed midday GPP reduction may be driven more by water stress than by direct ozone damage. At IT-BFt, the JULES-simulated GPP exhibits a sharp midday reduction, especially when ozone effects are included, suggesting a modelled compound stress due to high VPD and ozone uptake. However, the partitioned GPP at this site increases during the same period (after 10:00), indicating that stomatal closure due to VPD is not occurring to the extent the model assumes. This divergence suggests a potential overestimation of midday water limitation in the model configuration. At IT-Cp2, neither the modelled nor observed GPP shows a distinct midday dip, indicating that ozone and VPD effects are less pronounced or not synchronised enough to produce a compound stress response. These site-specific dynamics reinforce the need for a more accurate representation of stomatal regulation under co-occurring stresses in Mediterranean systems,

494

495

496

497

498

499

500

501

502

503

504

505

506

507

508

509

510

511

512

513

514

515

516

517

518

519

520

521

522

523

524

525

526

| | 10111atada: Cabeçanio |
|---|-----------------------|
| | |
| ١ | |
| | Formatou |

Cabacalha

Formatou

Formatou

Formatou
Formatou
Formatou
Formatou
Formatou
Formatou
Formatou
Formatou
Formatou

Formatou

Overall, these results reinforce the importance of including O₃ effects in GPP simulations, particularly in regions with high ozone exposure. While boreal sites show limited O₃ sensitivity, temperate and Mediterranean forests experience stronger reductions, necessitating careful model calibration to capture these interactions. The combination of ozone stress, VPD, and

latent heat flux (LE) amplifies these effects, further emphasising the need for site-specific parameter tuning.

In addition to evaluating RMSE and r², we examined residuals between observed and simulated GPP to identify systematic biases. At several sites, such as IT-BFt, residuals indicated that modelled GPP tended to underestimate peak values during high O₃ periods, particularly around midday. This aligns with the observed mismatch in diurnal dynamics (Fig. 6), suggesting that while optimisation improves overall fit, specific stress responses (e.g. compound O₃ and VPD effects) may still be underestimated or mistimed. These residual diagnostics support the need for further refinement in the representation of ozone damage under variable environmental conditions.

Table 45: Performance of optimised JULES without O3 and with O3 for O3 levels above 40 ppb for each site.

527

528 529

530

531 532

533

534

535

536

537

538 539

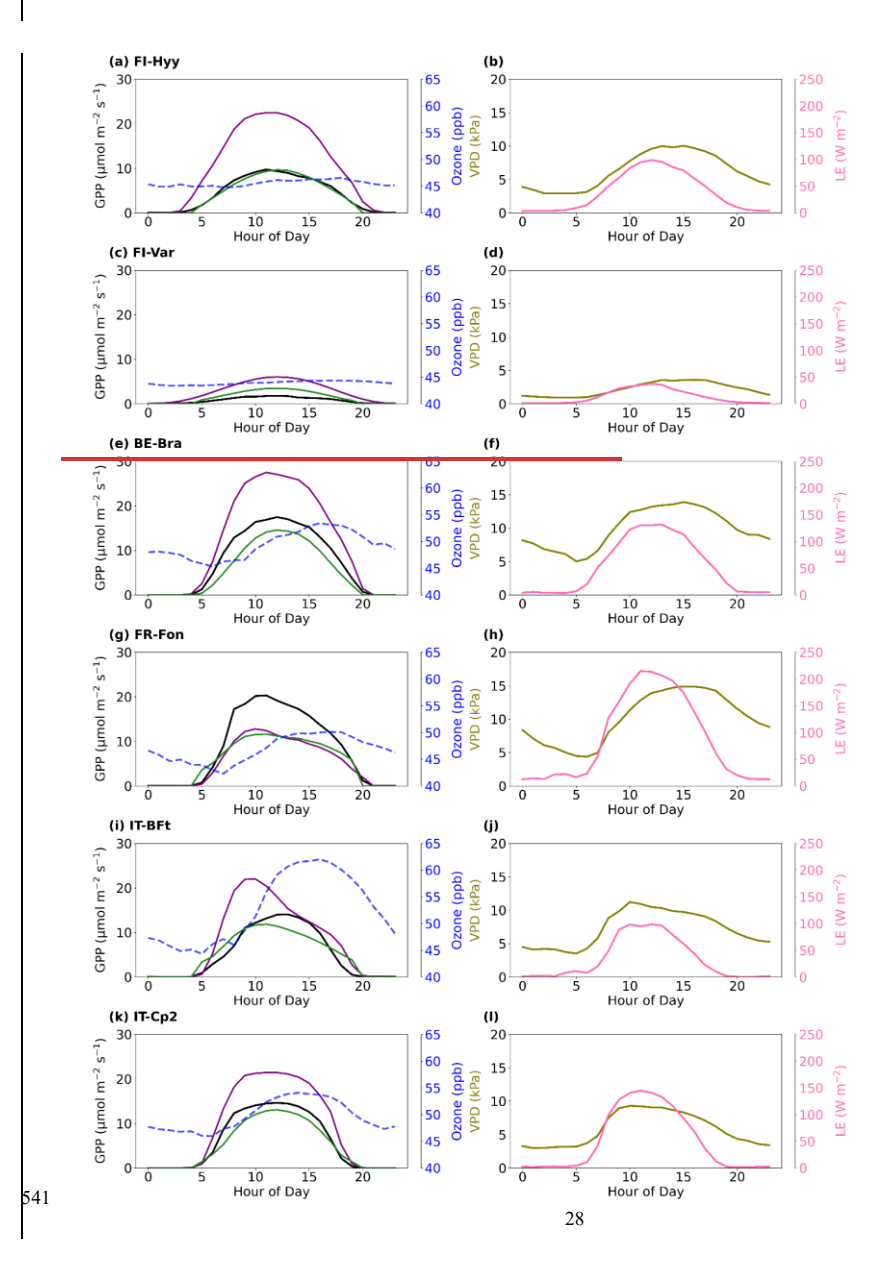
540

| | | FI- | FI- | FI- | FI- | BE- | BE- | FR- | J | FR- | IT. | | IT | <u>-</u> | IT- | IT- |
|-----|-------|------|----------------|------|----------------|------|----------------|------|------|------------|-----|------|----------------|-----------|------|----------------|
| | | Hyy | <u>Hyy</u> | Var | <u>Var</u> | Bra | <u>Bra</u> | Fon |] | <u>Fon</u> | BF | t | BI | <u>Ft</u> | Cp2 | <u>Cp2</u> |
| Met | rics | RMSE | \mathbf{r}^2 | RMSE | r ² | RMSE | r ² | RMS | SE 1 | r² | RM | 1SE | \mathbf{r}^2 | | RMSE | \mathbf{r}^2 |
| | Wit | 9.97 | 0.46 | 3.10 | 0.65 | 7.57 | 0.60 | 5.60 | 0.5 | 5 5 | .88 | 0.42 | 2 | 5.45 | 0.70 | |
| | hout | t | | | | | | | | | | | | | | |
| | O_3 | | | | | | | | | | | | | | | |
| | With | 0.52 | 0.85 | 1.18 | 0.70 | 3.09 | 0.73 | 5.47 | 0.5 | 9 2 | .31 | 0.6 | 5 | 1.93 | 0.77 | |
| | O_3 | | | | | | | | | | | | | | | |

Células Inseridas Células Inseridas Células Inseridas Células Inseridas Células Inseridas Células Inseridas Formatou: Tipo de letra: Negrito Formatada: Esquerda Formatada: Esquerda Formatada: Esquerda Formatada: Esquerda Formatada: Esquerda Formatada: Esquerda Formatou: Tipo de letra: Negrito Formatada: Esquerda Tabela Formatada

Formatada: Cabecalho







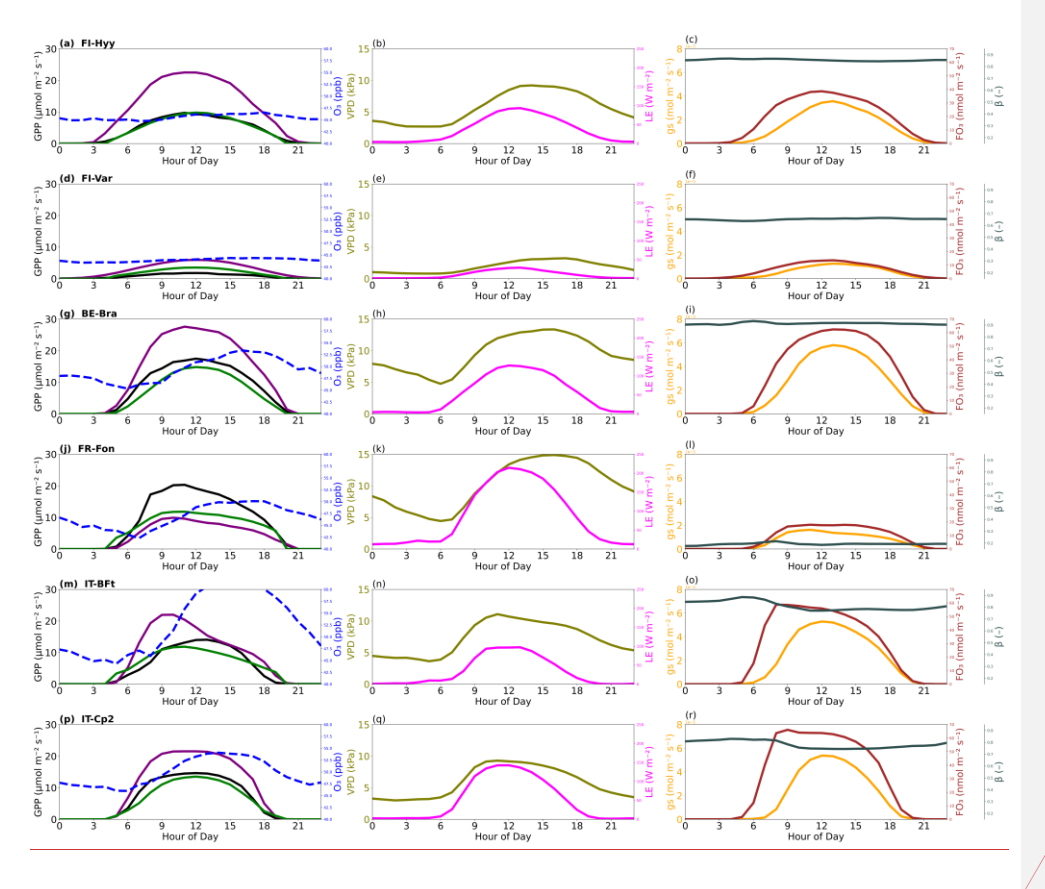


Figure 76: Averaged diurnal cycles of gross primary production (GPP₃), ozone (Θ₂), O₂), vapour pressure deficit (VPD), latent heat flux (LE), stomatal conductance (g₂), ozone flux into leaves (FO₃), and latent heat (LE the soil moisture limitation factor (β) across sites on high ozone days when ozone levels execeded(O₃ above 40 ppb) at six forest sites; (a₁ b₋₀) FI-Hyy, (c₂d₋) FI-Var, (c₇f₉₋₁) BE-Bra, (g₇h₋) FF-Fon, (i₇jm₋₀) IT-BFt, and (i₇jm₋₁) IT-Cp2, showing the . The left panels show observed GPP (black-line) and optimised simulated GPP from the optimised model without O₃ (purple-line) and with O₃ (green), O₃-concentration (Ozone, blue) at left column and vapour pressure deficit (along with ozone concentrations (blue dashed line). The middle panels show VPD₇ [olive] and LE (magenta). The right panels show g₂ (orange), FO₃ (brown), and latent heat flux (LE, pink) on the right column.β (dark slate grey)_a

Formatou: Cor do tipo de letra: Preto
Formatou: Inglês (Estados Unidos)

3.4 GPP reductions due to O3 effects

The mean annual GPP reduction varies significantly across the sites, suggesting a site-specific exposure and response to ozone stress (Fig. <u>87</u>). The negative values indicate a decrease in GPP, highlighting the impact of ozone as a stressor on plant productivity.

FI-Hyy and FI-Var show relatively small reductions in GPP, with annual mean decreases of -1.36 % and -1.04 %, respectively. This suggests that these northern sites are less sensitive to ozone stress, possibly due to lower background O₃ concentrations (Fig. 2, Table 1) or lower stomatal ozone uptake, which limits the damaging effects on GPP. In contrast, IT-BFt and IT-Cp2 exhibit the highest reductions (-6.2% and -5.4%, respectively), which can be attributed to higher ozone exposure (Fig. 2) and greater ozone uptake, exacerbating stress on photosynthesis and stomatal function. Similarly, temperate forests (BE-Bra and FR-Fon) exhibit moderate reductions in GPP, with declines of -5.22% and -2.62%, respectively. While ozone effects at FR-Fon are lower than those at BE-Bra, they are still significant, underscoring that broadleaf deciduous forests also experience ozone-induced productivity losses. The stronger impact at BE-Bra may be linked to higher stomatal ozone uptake, as suggested by the site's parameter sensitivity (Fig. 6).

These findings highlight the need for region-specific ozone mitigation strategies, particularly in Mediterranean ecosystems where ozone-induced reductions in GPP exceed _5_% annually. The combination of high ozone, VPD, and water stress in these regions may further amplify productivity losses, making them particularly vulnerable to future climate and air quality changes.

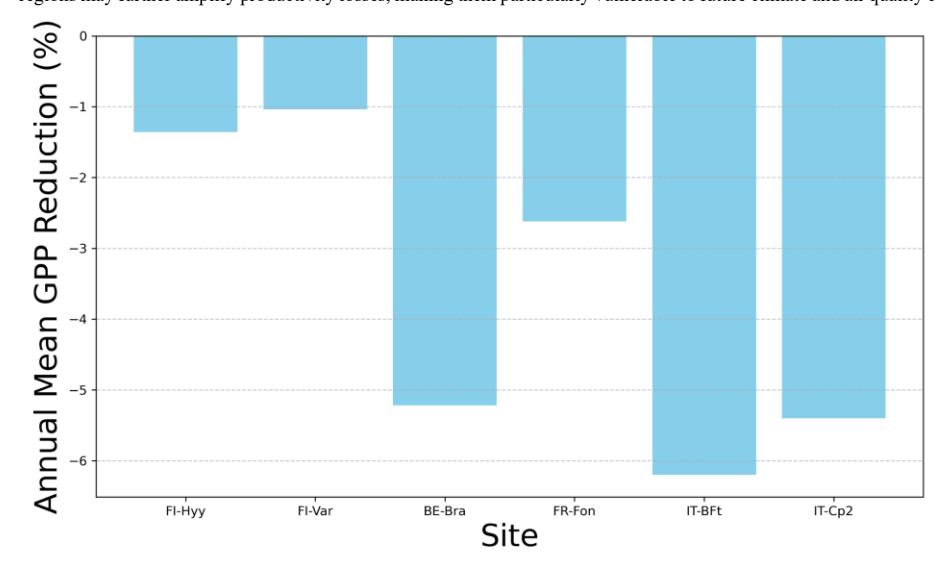


Figure 87: Annual mean GPP reduction due to ozone exposure (%). The bar plot represents the annual mean reduction in Gross Primary Productivity (GPP) as a percentage for each site: FI-Hyy, FI-Var, BE-Bra, FR-Fon, IT-BFt, and IT-Cp2.

4 Discussion and Conclusions

568

569

570

571

572

573

574

575

576

577

578

579

580

581

582

583

584

585

586

587

588

589

590

591

592

593

594

595

596

597

598

599

600

This study underscores the importance of incorporating ozone effects into the JULES model to enhance its accuracy in simulating Gross Primary Productivity (GPP) across diverse European forest ecosystems. By including ozone effects, the model demonstrated improved performance, particularly during high O3 events and in central and southern European sites where ozone stress is most pronounced. For example, reductions in RMSE at FR-Fon (from 9.53 to 5.71), IT-BFt (from 6.30 to 3.78), and IT-Cp2 (from 3.81 to 2.85) highlight the significant role of ozone in modulating plant productivity. These findings confirm previous observations that ozone exposure strongly influences plant photosynthesis and carbon sequestration, particularly in Mediterranean climates (Sitch et al., 2007). However, the minimal differences in northern European sites (FI-Hyy and FI-Var) suggest boreal forests' lower sensitivity to ozone, aligning with prior research showing lower ozone uptake in cooler, high-latitude environments (Wittig et al., 2009). The annual mean GPP reductions due to ozone exposure reveal a clear spatial gradient, with northern sites showing minimal reductions (-1.04% to -1.36%) and southern sites experiencing more pronounced decreases (-5.4% to -6.2%). This gradient reflects the interplay of higher ambient ozone concentrations, greater stomatal conductance, and compounding environmental stressors such as high temperatures and vapor pressure deficit in Mediterranean climates (Proietti et al., 2016). Central European sites (e.g., BE-Bra and FR-Fon) exhibited intermediate reductions, consistent with transitional climatic conditions that modulate ozone impacts. These patterns emphasise the importance of considering regional climatic variables in modeling ozone effects on GPP. For instance, Although Mediterranean species often exhibitmay possess physiological adaptations such as enhanced antioxidant production to mitigate ozone damage, thoughstress, such as conservative stomatal behaviour, these defenses can mechanisms may be overwhelmed insufficient under extremeconditions of sustained high ozone and environmental stress.

A key insight from our study is the potential overestimation of ozone impacts in prior modeling efforts. For example, Anav et al. (2011) estimated a 22% reduction in annual GPP across Europe using the ORCHIDEE model, while Oliver et al. (2018) simulated that GPP was reduced by 10 to 20% in temperate regions and by 2 to 8% in boreal regions using JULES. These discrepancies likely stem from differences in the resolution and accuracy of ozone and GPP datasets. By integrating high-resolution in situ ozone, meteorology, and GPP measurements, our study provides more precise estimates, reducing the biases inherent in purely simulation-based approaches. For instance, Gerosa et al. (2022) reported GPP reductions of 2.93% to 6.98% at IT-BFt using statistical models based on in situ data, aligning closely with our findings of a -6.2% GPP reduction. Similar conclusions were found by Conte et al. (2021), who adopted statistical models based on dynamic seasonal thresholds of ozone doses to reduce the bias between observed and modelled GPP_x-These results highlight the critical role of empirical data in refining model predictions.

This study's diurnal GPP, ozone, VPD, and LE patterns provide additional insights into the interaction between ozone and environmental stressors. Across all sites, ozone concentrations peaked in the late afternoon, coinciding with periods of high

Formatou: Cor do tipo de letra: Automática

VPD and LE. This temporal alignment underscoreshighlights the role of atmospheric conditions—such as, including high solar radiation and temperatures, in driving ozone formation and stomatal ozone uptake. Southern sites like, such as IT-BFt-and IT-Cp2, exhibited a pronounced midday declines decline in simulated GPP, reflecting their heightened modelled ozone sensitivity to ozone and the compounding effects interacting influence of high ozone concentrations and elevated VPD-and LE. However, the partitioned GPP at this site does not exhibit the same midday depression; instead, it increases gradually into the afternoon. At IT-Cp2, no midday dip is observed in either the simulated or observed GPP. These findings align with the work of Ainsworth et al. (2012), who demonstrated that multiple stressors can exacerbate the physiological impacts of ozone on plants. At BE-Bra, however, we observed a negative partial correlation between GPP and ozone (Section 3.1). Yet, the inclusion of ozone effects in the model resulted in only modest performance improvements. This contrast may arise from differences in timescale and model sensitivity. Verryckt et al. (2017), who conducted a detailed study at the same Scots pine stand, found no significant long-term GPP reduction attributable to ozone, despite frequent exceedance of critical exposure thresholds such as AOT40 and POD1. However, their residual analysis suggested short-term GPP reductions of up to 16% following days with high stomatal O₃ uptake, particularly in late spring and early summer. These results support the idea that ozone effects at BE-Bra may be episodic and confounded by co-occurring environmental stressors, such as light and temperature. The modest RMSE reduction in our simulations may thus reflect a structural limitation of the JULES damage formulation in capturing such short-lived physiological responses under temperate, humid conditions.

601

602

603

604

605

606

607

608

609

610

611

612

613

614

615

616

617

618

619

620

621

622

623

624

625

626

627

628

629

630

631

632

633

In contrast, boreal sites such as FI-Hyy exhibited minimal midday GPP reductions, consistent with their relative resilience to ozone stress under cooler atmospheric conditions. This supports prior research suggesting that boreal species often operate under a narrower range of stomatal conductance, limiting ozone uptake even during peak stress periods (Hoshika et al., 2013, Rannik et al., 2012). The variability in ozone impacts across sites emphasises the need for regional calibration of land surface models like JULES. This study optimised key parameters—, including the critical ozone flux, stomatal conductance sensitivity, and ozone sensitivity coefficient-to improve model performance. However, discrepancies at specific sites, such as, to improve model performance. While the results of this study are specific to the JULES model framework and the six European forest sites, some spatial trends, such as increasing ozone sensitivity (a) and decreasing critical ozone flux thresholds (FO3_{crit}) toward southern latitudes, may reflect broader physiological adaptations to environmental stress gradients. These patterns could inform the understanding of ozone responses in other forest ecosystems with comparable climatic and ecological conditions. However, we explicitly caution against the direct application of these site-calibrated parameter values to other regions without local validation, as species traits, soil properties, and climatic variability shape ozone responses. Notably, several of the physiological parameters optimised in this study, such as stomatal sensitivity (g₁), the photosynthetic capacity ratio (I_{max}: Vcmax), and the soil moisture stress threshold (p₀), are shared across multiple land surface and ecosystem models. This overlap suggests broader relevance, but these parameters must still be used with caution, as their values and effects can vary depending on the model structure. Although the quantitative results are JULES-specific, the methodological approach, site-level optimisation using in situ ozone and GPP data with a stomatal flux-based damage formulation, is transferable and could improve ozone-vegetation representation in other modelling frameworks.FR-Fon and IT-Cp2, indicate that further refinement

is necessary to capture local environmental conditions.

The JULES ozone damage scheme, as applied in this study, uses the instantaneous stomatal flux of ozone to compute a damage factor (F) that is applied equally to net photosynthesis (A) and stomatal conductance (g_p). This approach enables a simple and efficient integration into the model but may not fully capture the temporal dynamics of ozone-induced damage. Many other modeling frameworks use cumulative ozone uptake metrics—such as the phytotoxic ozone dose above a threshold (POD6)—to represent damage accumulation over time (Wittig et al., 2007; Lombardozzi et al., 2013). Moreover, empirical evidence indicates that A and g_p may respond differently to ozone, with distinct sensitivities and temporal responses (Lombardozzi et al., 2012a,b). Future versions of JULES could benefit from decoupling these effects by estimating separate sensitivity parameters (a) and critical thresholds (FO3_{crit}) for A and g_p, and by transitioning toward cumulative flux-based ozone stress formulations.

Our study highlights the importance of integrating long-term in situ measurements into land surface models to improve their accuracy and reliability. Expanding such measurements' spatial and temporal coverage is essential for capturing the full variability of ozone impacts across biomes and climatic conditions. Future research should also prioritise refining ozone response mechanisms in land surface models, particularly in regions where multiple stressors interact to influence plant productivity. For example, incorporating dynamic responses to heat waves, droughts, and other extreme events could provide a more comprehensive understanding of how ozone stress interacts with climate change.

Code Availability

JULES-vn7.4 was used for all simulations. The JULES model code and suite used to run the model are available from the Met Office Science Repository Service (MOSRS). Registration is required, and the code is available to anyone for non-commercial use (for details of licensing, see https://jules.jchmr.org/code, last access: 29 June 2024). Visit the JULES website (https://jules.jchmr.org/getting-started, last access: 29 June 2024) to register for a MOSRS account. Documentation for the JULES model is located at https://jules-lsm.github.io/vn7.4/ (last access: 29 June 2024). Site-level simulations used the rose suite u-dg903 (https://code.metoffice.gov.uk/trac/roses-u/browser/d/g/9/0/3, at revision 289677), which is a copy of the u-al752 JULES suite for FLUXNET 2015 and LBA sites described at https://code.metoffice.gov.uk/trac/jules/wiki/FluxnetandLbaSites (last access: 29 June 2024) and downloaded from https://code.metoffice.gov.uk/trac/roses-u/browser/a/1/7/5/2/ (Harper et al., 2021) at revision 286601. Suites can be downloaded from MOSRS once the user has registered for an account.

Formatada: Cabeçalho

Formatou: Tipo de letra: 10 pt

| Data Availability |
|---|
| The ICOS data (meteorological variables, fluxes and carbon dioxide concentration) used to run JULES are available for download from https://www.icos-cp.eu/observations (last access: 29 June 2024). The ozone data was obtained by requesting the PIs of each site, except Värriö, obtained through the SMEAR I research station (Kolari et al., 2024) and Hyytiälä, available |
| on SMEAR II Hyytiälä forest meteorology, greenhouse gases, air quality and soil dataset (Aalto et al., 2023). |
| Author contribution |
| IV wrote the paper and led the data analysis, with contributions from all authors. FM, SS, FB, PB, MB and HV contributed to the interpretation of the data. GG and SF contributed to in situ data for model evaluation. MCDR, SS and FB contributed to JULES simulations. |
| Competing interests |
| At least one of the (co-)authors is a member of the editorial board of Biogeosciences. |
| The authors declare that they have no conflict of interest. |
| Acknowledgements |
| IV was funded by Fonds Wetenschappelijk Onderzoek Flanders (FWO grant no. G018319N). FM was funded by the FWO as a senior postdoc and is thankful to this organisation for its financial support (FWO grant no. 1214723N). SS was funded through UKRI NERC funding (NE/R001812/1). MCDR has been supported by the H2020 4C project no. 821003, by the NetZeroPlus (NZ+) grant funded by UKRI-BBSRC award BB/V011588/1 and also by the UKRI-'AI for Net Zero' Programme project: ADD-TREES, Grant number EP/Y005597/1. The authors acknowledge Ivan Jansens from the University of Antwerp, Johan Neirynck from the Instituut Natuur- en Bosonderzoek, and Daniel Berveiller from the University of Paris-Saclay for the ozone datasets provided for the Brasschaat and Fontainebleau-Barbeau sites, respectively. |
| References |
| Aalto, J., Aalto, P., Keronen, P., Kolari, P., Rantala, P., Taipale, R., Kajos, M., Patokoski, J., Rinne, J., Ruuskanen, T., Leskinen, M., Laakso, H., Levula, J., Pohja, T., Siivola, E., Kulmala, M., & Ylivinkka, I.: SMEAR II Hyytiälä forest meteorology, greenhouse gases, air quality and soil. University of Helsinki, Institute for Atmospheric and Earth System |

Formatada: Cabeçalho

Research. https://doi.org/10.23729/23dd00b2-b9d7-467a-9cee-b4a122486039, 2023.

- Ainsworth, E. A., Lemonnier, P., and Wedow, J. M.: The influence of rising tropospheric carbon dioxide and ozone on plant productivity, Plant Biol., 21, 59-71, 2019.
- Ainsworth, E. A., Yendrek, C. R., Sitch, S., Collins, W. J., and Emberson, L. D.: The effects of tropospheric ozone on net primary productivity and implications for climate change, Annu. Rev. Plant Biol., 63, 637-661, 2012.
- Anav, A., Menut, L., Khvorostyanov, D., and Viovy, N.: Impact of tropospheric ozone on the Euro-Mediterranean vegetation,
- Glob. Change Biol., 17, 2342–2359, https://doi.org/10.1111/j.1365-2486.2010.02387.x, 2011.
- Anav, A., De Marco, A., Proietti, C., Alessandri, A., Dell'Aquila, A., Cionni, I., Friedlingstein, P., Khvorostyanov, D., Menut,
 L., Paoletti, E., Sicard, P., Sitch, S., & Vitale, M.: Comparing concentration-based (AOT40) and stomatal uptake (PODY)
 - L., Paoletti, E., Sicard, P., Sitch, S., & Vitale, M.: Comparing concentration-based (AOT40) and stomatal uptake (PODY) metrics for ozone risk assessment to European forests, Global Change Biology, 22, https://doi.org/10.1111/gcb.13138, 2016.
- 701 Best, M. J., Pryor, M., Clark, D. B., Rooney, G. G., Essery, R. L. H., Ménard, C. B., Edwards, J. M., Hendry, M. A., Porson,
- 702 A., Gedney, N., Mercado, L. M., Sitch, S., Blyth, E., Boucher, O., Cox, P. M., Grimmond, C. S. B., and Harding, R. J.: The
- 703 Joint UK Land Environment Simulator (JULES), model description Part 1: Energy and water fluxes, Geosci. Model Dev.,
- 704 4, 677–699, https://doi.org/10.5194/gmd-4-677-2011, 2011.
 - Cailleret, M., Ferretti, M., Gessler, A., Rigling, A., & Schaub, M.: Ozone effects on European forest growth—Towards an
- 707 integrative approach, Journal of Ecology, 106, 1377 1389. https://doi.org/10.1111/1365-2745.12941, 2018.
- 709 Clark, D. B., Mercado, L. M., Sitch, S., Jones, C. D., Gedney, N., Best, M. J., Pryor, M., Rooney, G. G., Essery, R. L. H.,
- P10 Blyth, E., Boucher, O., Harding, R. J., Huntingford, C., and Cox, P. M.: The Joint UK Land Environment Simulator (JULES),
- 711 model description Part 2: Carbon fluxes and vegetation dynamics, Geosci. Model Dev., 4, 701-722,
- 712 https://doi.org/10.5194/gmd-4-701-2011, 2011.

690

693

699 700

705 706

708

713

716

- 714 Clifton, O. E., Fiore, A. M., Correa, G., Horowitz, L. W., and Naik, V.: Effects of regional climate change on air quality across
- the United States: a review of dynamic modeling studies, Environ. Res. Lett., 15, 123007, 2020.
- 717 Conte, A., Otu-Larbi, F., Alivernini, A., Hoshika, Y., Paoletti, E., Ashworth, K., & Fares, S.: Exploring new strategies for
- 718 ozone-risk assessment: A dynamic-threshold case study. Environmental Pollution, 287, 117620.
- 719 https://doi.org/10.1016/j.envpol.2021.117620, 2021.

- 721 Dengel, S., Grace, J., Aakala, T., Hari, P., Newberry, S. L., and Mizunuma, T.: Spectral characteristics of pine needles at the
- 722 limit of tree growth in subarctic Finland, Plant Ecol. Divers., 6, 31–44, https://doi.org/10.1080/17550874.2012.754512, 2013.
- 724 Ducker, J., Muller, J. B., Whalley, L. K., Parker, A. E., and Oetjen, H.: The impact of leaf physiology on the ozone flux of an
 - urban woodland, Agric. For. Meteorol., 252, 51-63, 2018.
- 727 Emberson, L. D., Ashmore, M. R., Cambridge, H. M., Simpson, D., and Tuovinen, J. P.: Modelling stomatal ozone flux across
- 728 Europe, Water Air Soil Pollut., 130, 577-582, 2001.
- 729
- 730 Farquhar, G. D., von Caemmerer, S., and Berry, J. A.: A biochemical model of photosynthetic CO2 assimilation in leaves of
- 731 C₃ species, Planta, 149, 78–90, https://doi.org/10.1007/BF00386231, 1980.
- 733 Feng, Z., Xu, Y., Kobayashi, K., Dai, L., Zhang, T., Agathokleous, E., Calatayud, V., Paoletti, E., Mukherjee, A., Agrawal,
- 734 M., Park, R. J., Oak, Y. J., and Yue, X.: Ozone pollution threatens the production of major staple crops in East Asia, Nat. Food,
- 735 3, 47–56, https://doi.org/10.1038/s43016-021-00422-6, 2022.
- 737 Fowler, D., Coyle, M., Skiba, U., Sutton, M. A., Cape, J. N., Reis, S., Sheppard, L. J., Jenkins, A., Grizzetti, B., Galloway, J.
- 738 N., Vitousek, P., Leach, A., Bouwman, A. F., Butterbach-Bahl, K., Dentener, F., Stevenson, D., Amann, M., and Voss, M.:
- The global nitrogen cycle in the twenty-first century, Philos. Trans. R. Soc. B Biol. Sci., 368, 20130164, 2009.
- 741 Gerosa, G. A., Marzuoli, R., and Finco, A.: Interannual variability of ozone fluxes in a broadleaf deciduous forest in Italy,
- 742 Elementa: Sci. Anthrop., 10(1), doi:10.1525/elementa.2021.00105, 2022.
 - Gielen, B., Vandermeiren, K., Serneels, R., Valcke, R., and Ceulemans, R.: Ozone stress in young trees: Effects on
- photosynthesis, leaf area and root biomass allocation, Tree Physiol., 27, 123-131, 2007.
- 747 Gratani, L., and Crescente, M. F.: Map-making of plant biomass and leaf area index for management of protected areas, Aliso:
- 748 A Journal of Systematic and Floristic Botany, 19, 13-24, https://scholarship.claremont.edu/aliso/vol19/iss1/2, 2000.
- 750 Grulke, N., & Heath, R.: Ozone effects on plants in natural ecosystems. Plant biology, https://doi.org/10.1111/plb.12971,
- 751 2019.

723

725

726

732

736

740

743 744

746

749

752

- 753 Harper, A. B., Cox, P. M., Friedlingstein, P., Wiltshire, A. J., Jones, C. D., Sitch, S., Mercado, L. M., Groenendijk, M.,
 - Robertson, E., Kattge, J., Bönisch, G., Atkin, O. K., Bahn, M., Cornelissen, J., Niinemets, Ü., Onipchenko, V., Peñuelas, J.,

- 755 Poorter, L., Reich, P. B., Soudzilovskaia, N. A., and Bodegom, P. V.: Improved representation of plant functional types and
- 756 physiology in the Joint UK Land Environment Simulator (JULES v4.2) using plant trait information, Geosci. Model Dev., 9,
 - 2415-2440, https://doi.org/10.5194/gmd-9-2415-2016, 2016.
- 758
- Harper, A. B., Williams, K. E., McGuire, P. C., Duran Rojas, M. C., Hemming, D., Verhoef, A., Huntingford, C., Rowland,
 - L., Marthews, T., Breder Eller, C., Mathison, C., Nobrega, R. L. B., Gedney, N., Vidale, P. L., Otu-Larbi, F., Pandey, D.,
 - Garrigues, S., Wright, A., Slevin, D., De Kauwe, M. G., Blyth, E., Ardö, J., Black, A., Bonal, D., Buchmann, N., Burban, B.,
 - Fuchs, K., de Grandcourt, A., Mammarella, I., Merbold, L., Montagnani, L., Nouvellon, Y., Restrepo-Coupe, N., and
- 763 Wohlfahrt, G.: Improvement of modeling plant responses to low soil moisture in JULESvn4.9 and evaluation against flux
 - tower measurements, Geosci. Model Dev., 14, 3269-3294, https://doi.org/10.5194/gmd-14-3269-2021, 2021.
 - Harper, A., Williams, K., McGuire, P. C., Duran Rojas, C., and Otu-Larbi, F.: Rose suite u-al752, MetOffice [code],
 - https://code.metoffice.gov.uk/trac/roses-u/browser/a/1/7/5/2/trunk, last access: 29 June 2024.
- Hoshika, Y., Watanabe, M., Inada, N., & Koike, T.: Model-based analysis of avoidance of ozone stress by stomatal closure in
- 770 Siebold's beech (Fagus crenata).. Annals of botany, 112 6, 1149-58. <u>https://doi.org/10.1093/aob/mct166</u>, 2013.
- Hoshika, Y., Fares, S., Pellegrini, E., Conte, A., & Paoletti, E.: Water use strategy affects avoidance of ozone stress by stomatal
 - closure in Mediterranean trees -A modelling analysis, Plant, cell & environment, https://doi.org/10.1111/pce.13700, 2019;
 - Jarvis, P. G.: The interpretation of the variations in leaf water potential and stomatal conductance found in canopies in the
- 776 field, Philos. Trans. R. Soc. Lond. B Biol. Sci., 273, 593-610, 1976.
- 778 Kangasjarvi, J., Jaspers, P., Kollist, H., and Brosche, M.: Mechanisms of plant responses to ozone, Biol. Plant., 49, 5-19, 2005.
- 779 Kolari, P., Dengel, S., Peltola, O., Sahoo, G., & Siivola, E.: SMEAR I Värriö forest eddy covariance. University of Helsinki,
- 780 Institute for Atmospheric and Earth System Research. https://doi.org/10.23729/6dd3e1bf-22f3-4f83-aed3-a39da5181d29,
- 781 2024.

757

760

761 762

764

765 766

767 768

771

773

774 775

777

782

- Lee, J.-E., Frankenberg, C., van der Tol, C., Berry, J. A., Guanter, L., Boyce, C. K., Fisher, J. B., Morrow, E., Worden, J. R.,
- 784 Asefi, S., Badgley, G., and Saatchi, S.: Forest productivity and water stress in Amazonia: observations from GOSAT
- 785 <u>chlorophyll fluorescence, Proc. R. Soc. B, 280, 20130171, https://doi.org/10.1098/rspb.2013.0171, 2013.</u>
- Li, P., Feng, Z., and Paoletti, E.: A meta-analysis on growth, physiological, and biochemical responses of woody species to
- 788 tropospheric ozone, Environ. Pollut., 244, 322-331, 2019.

Li, Y., Zhang, W., Wang, X., and Tian, Y.: Effects of ozone on carbon cycling and sequestration in terrestrial ecosystems: A review. Sci. Total Environ.. 838. 156316, 2022.

Lin, M., Malyshev, S., Shevliakova, E., Paulot, F., Horowitz, L. W., Fares, S., Mikkelsen, T. N., and Zhang, L.: Sensitivity of ozone dry deposition to ecosystem–atmosphere interactions: A critical appraisal of observations and simulations, Glob.

795 <u>Biogeochem. Cycles</u>, 33, 1264–1288, https://doi.org/10.1029/2018GB006157, 2019.

Lombardozzi, D., Levis, S., Bonan, G., and Sparks, J. P.: Predicting photosynthesis and transpiration responses to ozone: decoupling modeled photosynthesis and stomatal conductance, Biogeosciences, 9, 3113–3130, https://doi.org/10.5194/bg-9-3113-2012, 2012.

Lombardozzi, D., S. Levis, G. Bonan, P. G. Hess, and J. P. Sparks, 2015: The Influence of Chronic Ozone Exposure on Global Carbon and Water Cycles. J. Climate, 28, 292–305, https://doi.org/10.1175/JCLI-D-14-00223.1.

Lu, J., Yao, L.: Observational evidence for detrimental impact of inhaled ozone on human respiratory system. BMC Public Health 23, 929, https://doi.org/10.1186/s12889-023-15902-6, 2023

Lu, X., Zhang, L., and Chen, Y.: Interactions between urbanisation, economic development and air pollution in China: Evidence from dynamic simultaneous equations models, J. Clean. Prod., 212, 1468-1480, 2019.

Liu, D. C., and Nocedal, J.: On the limited memory BFGS method for large scale optimisation, Math. Program., 45, 503–528, https://doi.org/10.1007/BF01589116, 1989.

- Medlyn, B. E., Duursma, R. A., Eamus, D., Ellsworth, D. S., Prentice, I. C., Barton, C. V. M., Crous, K. Y., de Angelis, P., Freeman, M., and Wingate, L.: Reconciling the optimal and empirical approaches to modelling stomatal conductance, Glob.
- 815 Change Biol., 17, 2134–2144, https://doi.org/10.1111/j.1365-2486.2010.02375.x, 2011.

- Nuvolone, D., Petri, D., and Voller, F.: The effects of ozone on human health, Environ. Sci. Pollut. Res., 25, 175-196,
- 818 https://doi.org/10.1007/s11356-017-9239-3, 2018.

820 Oli

- Oliver, R. J., Mercado, L. M., Clark, D. B., Huntingford, C., Taylor, C. M., Vidale, P. L., McGuire, P. C., Todt, M., Folwell,
- 821 S., Shamsudheen Semeena, V., and Medlyn, B. E.: Improved representation of plant physiology in the JULES-vn5.6 land

- 822 surface model: photosynthesis, stomatal conductance and thermal acclimation, Geosci. Model Dev., 15, 5567-5592,
- 823 https://doi.org/10.5194/gmd-15-5567-2022, 2022.
- 825 Oliver, R. J., Mercado, L. M., Sitch, S., Simpson, D., Medlyn, B. E., Lin, Y.-S., and Folberth, G. A.: Large but decreasing
- effect of ozone on the European carbon sink, Biogeosciences, 15, 4245–4269, https://doi.org/10.5194/bg-15-4245-2018, 2018.
- 828 Op de Beeck, M., Gielen, B., Jonckheere, I., Samson, R., Janssens, I. A., and Ceulemans, R.: Needle age-related and seasonal
 - photosynthetic capacity variation is negligible for modelling yearly gas exchange of a sparse temperate Scots pine forest,
- 830 Biogeosciences, 7, 199–215, https://doi.org/10.5194/bg-7-199-2010, 2010.
- 0tu-Larbi, F., Conte, A., Fares, S., Wild, O., and Ashworth, K.: Current and future impacts of drought and ozone stress on
- Northern Hemisphere forests, Glob. Change Biol., 26, 6218–6234, https://doi.org/10.1111/gcb.15339, 2020.
- 835 Proietti, C., Anav, A., and De Marco, A.: The contribution of stomatal and non-stomatal pathways to ozone flux in different
- 836 European forests, Sci. Total Environ., 799, 149326, 2021.
- 838 Proietti, C., Anav, A., Anav, A., Marco, A., Sicard, P., & Vitale, M.: A multi-sites analysis on the ozone effects on Gross
- 839 Primary Production of European forests, The Science of the total environment, 556, 1-11 .
- 840 <u>https://doi.org/10.1016/j.scitotenv.2016.02.187</u>, 2016.
- 842 Rannik, Ü., Altimir, N., Mammarella, I., Bäck, J., Rinne, J., Ruuskanen, T., Hari, P., Vesala, T., & Kulmala, M.: Ozone
- 843 deposition into a boreal forest over a decade of observations: evaluating deposition partitioning and driving variables.
- 844 Atmospheric Chemistry and Physics, 12, 12165-12182. https://doi.org/10.5194/ACP-12-12165-2012, 2012.
- 846 Savi, F., Nemitz, E., Coyle, M., Aitkenhead, M., Frumau, K., Gerosa, G., Finco, A., Gruening, C., Goded, I., Loubet, B., Stella,
- P., Ruuskanen, T., Weidinger, T., Horvath, L., Zenone, T., and Fares, S.: Neural network analysis to evaluate ozone damage
- to vegetation under different climatic conditions, Front. For. Glob. Change, 3, 42, https://doi.org/10.3389/ffgc.2020.00042,
- 849 2020.

824

827

829

831

834

837

841

845

850

- 851 Schraik, D., Wang, D., Hovi, A., and Rautiainen, M.: Quantifying stand-level clumping of boreal, hemiboreal and temperate
- 852 European forest stands using terrestrial laser scanning, Agric. For. Meteorol., 339, 109564,
- 853 doi:10.1016/j.agrformet.2023.109564, 2023.

- 855 Sellar, A. A., Jones, C. G., Mulcahy, J. P., Tang, Y., Yool, A., Wiltshire, A., O'Connor, F. M., Stringer, M., Hill, R., Palmieri,
- J., Woodward, S., de Mora, L., Kuhlbrodt, T., Rumbold, S. T., Kelley, D. I., Ellis, R., Johnson, C. E., Walton, J., Abraham, N.
 - L., Andrews, M. B., Andrews, T., Archibald, A. T., Berthou, S., Burke, E., Blockley, E., Carslaw, K., Dalvi, M., Edwards, J.,
- 858 Folberth, G. A., Gedney, N., Griffiths, P. T., Harper, A. B., Hendry, M. A., Hewitt, A. J., Johnson, B., Jones, A., Jones, C. D.,
- 859 Keeble, J., Liddicoat, S., Morgenstern, O., Parker, R. J., Predoi, V., Robertson, E., Siahaan, A., Smith, R. S., Swaminathan,
- 860 R., Woodhouse, M. T., Zeng, G., and Zerroukat, M.: UKESM1: Description and Evaluation of the U.K. Earth System Model,
- 861 J. Adv. Model. Earth Sy., 11, 4513–4558, https://doi.org/10.1029/2019MS001739, 2019.
- 863 Shang, B., Agathokleous, E., Calatayud, V., Peng, J., Xu, Y., Li, S., Liu, S., & Feng, Z.: Drought mitigates the adverse effects
- 864 of O3 on plant photosynthesis rather than growth: A global meta-analysis considering plant functional types, Plant, cell &
- 865 environment, https://doi.org/10.1111/pce.14808, 2024.
- 867 Sicard, P., De Marco, A., Dalstein-Richier, L., Tagliaferro, F., Renou, C., & Paoletti, E.: An epidemiological assessment of
 - stomatal ozone flux-based critical levels for visible ozone injury in Southern European forests, The Science of the total
- 869 environment, 541, 729-741 . https://doi.org/10.1016/j.scitotenv.2015.09.113, 2016.
- 871 Sitch, S., Cox, P. M., Collins, W. J., and Huntingford, C.: Indirect radiative forcing of climate change through ozone effects
 - on the land-carbon sink, Nature, 448, 791-794, https://doi.org/10.1038/nature06059, 2007.
- 874 Sorrentino, B., Anav, A., Calatayud, V., Collalti, A., Sicard, P., Leca, S., Fornasier, F., Paoletti, E., and De Marco, A.:
 - Inconsistency between process-based model and dose–response function in estimating biomass losses in Northern Hemisphere
- due to elevated O₃, Environ. Pollut., 364, 125379, https://doi.org/10.1016/j.envpol.2024.125379, 2025.
- 878 Soudani, K., Delpierre, N., Berveiller, D., Hmimina, G., Pontailler, J.-Y., Seureau, L., Vincent, G., and Dufrêne, É.: A survey
- of proximal methods for monitoring leaf phenology in temperate deciduous forests, Biogeosciences, 18, 3391-3408,
- 880 https://doi.org/10.5194/bg-18-3391-2021, 2021.
- 882 Verryckt, L., Beeck, M., Neirynck, J., Gielen, B., Roland, M., & Janssens, I.:. No impact of tropospheric ozone on the gross
- primary productivity of a Belgian pine forest. Biogeosciences, 14, 1839-1855, https://doi.org/10.5194/BG-14-1839-2017,
- 884 2017.

857

862

866

868

870

872

873

875

877

881

- 886 Vallat, R.. Pingouin: statistics in Python. Journal of Open Source Software, 3(31), 1026, https://doi.org/10.21105/joss.01026,
- 887 2018.

| 891 | https://doi.org/10.1016/j.atmosenv.2008.10.033, 2009. | | | | | |
|-----|--|--|--|--|--|--|
| 892 | | | | | | |
| 893 | Vargas, R., Sonnentag, O., Abramowitz, G., Carrara, A., Chen, J., Ciais, P., Correia, A., Keenan, T., Kobayashi, H., Ourcival, | | | | | |
| 894 | J., Papale, D., Pearson, D., Pereira, J., Piao, S., Rambal, S., & Baldocchi, D.: Drought Influences the Accuracy of Simulated | | | | | |
| 895 | Ecosystem Fluxes: A Model-Data Meta-analysis for Mediterranean Oak Woodlands. Ecosystems, 16, 749-764. | | | | | |
| 896 | https://doi.org/10.1007/s10021-013-9648-1, 2013. | | | | | |
| 897 | | | | | | |
| 898 | Warm Winter 2020 Team, ICOS Ecosystem Thematic Centre.: Warm Winter 2020 ecosystem eddy covariance flux product | | | | | |
| 899 | for 73 stations in FLUXNET-Archive format—release 2022-1 (Version 1.0). ICOS Carbon Portal. | | | | | |
| 900 | https://doi.org/10.18160/2G60-ZHAK, 2022. | | | | | |
| 901 | | | | | | |
| 902 | Wittig, V., Ainsworth, E., Naidu, S., Karnosky, D., & Long, S.: Quantifying the impact of current and future tropospheric | | | | | |
| 903 | ozone on tree biomass, growth, physiology and biochemistry: a quantitative meta-analysis. Global Change Biology, 15. | | | | | |
| 904 | https://doi.org/10.1111/j.1365-2486.2008.01774.x, 2009. | | | | | |
| 905 | | | | | | |
| 906 | Wong, T. J., Roy, A., and Lefer, B. L.: Estimating biogenic VOC emissions from leaf, branch, and canopy scale measurements | | | | | |
| 907 | in an urban park, Atmos. Environ., 254, 118347, 2022. | | | | | |
| 908 | Yue, X. and Unger, N.: Ozone vegetation damage effects on gross primary productivity in the United States, Atmos. Chem. | | | | | |
| 909 | Phys., 14, 9137–9153, https://doi.org/10.5194/acp-14-9137-2014, 2014. | | | | | |
| 910 | | | | | | |
| 911 | Zhang, L., Brook, J. R., and Vet, R.: A revised parameterization parameterization for gaseous dry deposition in air-quality | | | | | |
| 912 | models, Atmos. Chem. Phys., 3, 2067–2082, https://doi.org/10.5194/acp-3-2067-2003, 2003. | | | | | |
| 913 | | | | | | |
| 914 | Zhu, L., Zhao, W., Ma, X., and Li, H.: Effects of ozone pollution on crop yields and economic losses in China, Environ. Pollut., | | | | | |
| 915 | 305, 119267, 2022. | | | | | |
| | | | | | | |
| | | | | | | |

Van Dingenen, R., Dentener, F. J., Raes, F., Krol, M. C., Emberson, L., and Muller, J. F.: The global impact of ozone on

agricultural crop yields under current and future air quality legislation, Atmos. Environ., 43, 604-618,

889 890